

| ADVANCED REVIEW OPEN ACCESS

Embedded Many-Body Green's Function Methods for Electronic Excitations in Complex Molecular Systems

Gianluca Tirimbó^{1,2} | Vivek Sundaram^{1,2,3} | Björn Baumeier^{1,2} 

¹Department of Mathematics and Computer Science, Eindhoven University of Technology, Eindhoven, The Netherlands | ²Institute for Complex Molecular Systems, Eindhoven University of Technology, Eindhoven, The Netherlands | ³Department of Applied Physics and Science Education, Eindhoven University of Technology, Eindhoven, The Netherlands

Correspondence: Björn Baumeier (b.baumeier@tue.nl)

Received: 7 June 2024 | **Revised:** 17 September 2024 | **Accepted:** 4 October 2024

Edited by: Peter R. Schreiner, Editor-in-Chief

Funding: This work was supported by Exacte en Natuurwetenschappen, Joint CSER and eScience Program for Energy Research, Vidi 723.016.002.

Keywords: electronic excitations | embedding | excitons | Greens Functions | quasiparticles

ABSTRACT

Many-body Green's function theory in the *GW* approximation with the Bethe–Salpeter equation (BSE) provides a powerful framework for the first-principles calculations of single-particle and electron–hole excitations in perfect crystals and molecules alike. Application to complex molecular systems, for example, solvated dyes, molecular aggregates, thin films, interfaces, or macromolecules, is particularly challenging as they contain a prohibitively large number of atoms. Exploiting the often localized nature of excitation in such disordered systems, several methods have recently been developed in which *GW*-BSE is applied to a smaller, tractable region of interest that is embedded into an environment described with a lower-level method. Here, we review the various strategies proposed for such embedded many-body Green's functions approaches, including quantum–quantum and quantum–classical embeddings, and focus in particular on how they include environment screening effects either intrinsically in the screened Coulomb interaction in the *GW* and BSE steps or via extrinsic electrostatic couplings.

1 | Introduction

The controlled use of electronic excitations in materials has led to important technological advancements, such as the design of cutting-edge optoelectronic devices and the development of energy-efficient materials. Understanding electronic excitations is crucial for unlocking the full potential of materials, and ab initio methods offer insight into these quantum-level processes without requiring extensive experimental input. However, as materials become more complex, with thousands or even millions of atoms, and real-world conditions come into play, accurately simulating these systems becomes a significant computational challenge. Macroscopic phenomena like optical absorption, luminescence, electrical conductivity, and other bulk or surface material properties cannot be fully captured by

microscale models alone due to the complex interactions across larger lengths and time scales. As a result, studying electronic excitations in complex disordered systems remains a challenge for ab initio methods.

Many-Body Green's Functions Theory in the *GW* approximation and Bethe–Salpeter Equation (BSE) has often been considered the method of choice for the calculation of electronically excited states (both charged and neutral) in hard condensed matter systems [1–3], starting from a mean-field ground-state reference often obtained from density functional theory [4, 5] (DFT). Early studies in the late 1990s of inorganic crystals such as elementary semiconductors, or insulators such as magnesium oxide or lithium fluoride have been tractable because the atomic structure of these materials can be represented by small unit cells with

This is an open access article under the terms of the [Creative Commons Attribution License](#), which permits use, distribution and reproduction in any medium, provided the original work is properly cited.

© 2024 The Author(s). *WIREs Computational Molecular Science* published by Wiley Periodicals LLC.

only a few atoms [6]. Nowadays, efficient implementations with periodic boundary conditions (PBCs) [7–10] coupled with recent methodological developments [11, 12] and increased computing power have allowed treating larger systems, such as reconstructed surfaces, defect structures, or in general materials with more complex structures [13, 14].

At the other end of the material spectrum, interest in applying *GW*-BSE to study molecular excitations has picked up considerably later, beginning in earnest around 2010. The possible explanations for this delayed uptake are likely pragmatic: (i) many-body wave function-based quantum chemistry alternatives such as coupled-cluster or configuration interaction have widely been, and still are, considered the state-of-the-art [15–17], and (ii) existing *GW*-BSE implementations in solid-state codes with PBCs and a plane-wave basis are rather inefficient for isolated systems, requiring large and mostly empty unit cells. With implementations without PBCs and localized-orbital bases instead of plane waves becoming available, several groups showed that Green's function methods are very powerful also in molecular systems, balancing—simplified speaking—the accuracy of more computationally expensive wave function methods with the cost of time-dependent density-functional theory [18] (TDDFT). One of the most notorious problems, for instance, of TDDFT is the very sensitive dependence of predicted charge-transfer type excitation energies on the choice of the exchange-correlation functional [19]. In *GW*-BSE these excitation energies are predicted with the same accuracy as localized excitations (compared with the experiment) usually without the need for special tuning [20–22].

Based on these and more [23–28] promising results for various types of excitations in single molecules or dimers, it is natural to turn the attention to more complex material systems, such as solvated dyes, molecular aggregates, thin films, interfaces, or macromolecules. However, as for all other ab initio methods, the system sizes required to realistically and representatively study electronic excitations in such materials exceed by far what is computationally tractable. Yet, the realization that many of such material systems are characterized by a significant amount of disorder leading to—in broad terms—localization of electronic states (in contrast to the Bloch states in hard condensed matter), offers a way out of this conundrum. That is, partitioning the overall system into a region of interest (“active region”), say a dye molecule, which is embedded in a surrounding region such as one containing a solvent. Both regions can then be described at different levels of theory such that the very accurate and computationally expensive method is restricted to the active region, while a less expensive lower-level method is used for the environment. This lower level can be either a simplified quantum mechanical (QM) model in a QM/QM setting [29–31], a molecular mechanics (MM) approach (QM/MM) [32], or a continuum model [33–35] representing the environment as a structure-less material having realistic macroscopic dielectric properties.

In the context of all of these approaches, the focus of this topical review is specifically on embedded Many-Body Green's Function methods, that is, calculations using *GW*-BSE as the high-accuracy electronic structure method for a region of interest embedded into a region at lower-level description. As we will see, there are generally two classes of embedding strategies here: one treats *GW*-BSE just as any other high-level method and

couples it *extrinsically* to the lower-level method via, for example, in the case of only weakly interacting systems, purely classical electrostatic interaction modules. While very powerful, as we will discuss in detail in Section 3.3, *GW*-BSE also allows for another class of approaches. These exploit the fact that one of the main ingredients of Green's functions methods here is the screened Coulomb interaction, *W*, which is essential for representing the electronic many-body effects in quasiparticle and electron–hole excitations. In some sense, *GW*-BSE can be seen as an exciting merger between advanced quantum-mechanical principles, on the one hand, with classical electrostatic concepts, on the other hand. Embedding approaches can be devised that explicitly and *intrinsically* make use of these electrostatic concepts at the core of *GW*-BSE.

In this review, we will in the following first briefly revisit the general methodology of *GW*-BSE in Section 2 to introduce the main concepts and equations as well as some computational aspects as they will be relevant later. Section 3 is devoted to the discussion of the various embedding strategies, starting from *GW*-BSE-in-DFT methods either starting from projection-based-embedding or subsystem DFT, introducing approximations to *GW*-BSE-in-MM embedding, and different flavors of external *GW*-BSE/MM calculations. For each of these approaches, we will summarize the main theoretical aspects and some computational details. Throughout, we will also give a few examples of application to material systems, ranging from small dimer complexes, via solvent-solute systems, to molecular films and surfaces.

2 | Many-Body Green's Functions Methods for Electronically Excited States

In this section, we briefly recapitulate the essential ideas and theoretical framework of Green's functions approaches, upon which the embedding methods we will discuss are based. We restrict ourselves to the discussion of the most important results and refer the interested reader to more exhaustive derivations in the literature [3].

All the following are essential approaches to extracting information on the excited states of a system consisting of *M* nuclei and *N* electrons. The coordinates \mathbf{R}_α of the individual nuclei with charges Z_α and \mathbf{r}_i of the individual electrons are combined into the variables $\bar{\mathbf{R}} = (\mathbf{R}_1, \mathbf{R}_2, \dots, \mathbf{R}_M)$ and $\bar{\mathbf{r}} = (\mathbf{r}_1, \mathbf{r}_2, \dots, \mathbf{r}_N)$, respectively. For a simpler presentation, we consider a system with a spin-singlet, closed-shell ground state. Hartree atomic units are used throughout. Using the Born–Oppenheimer separation with the adiabatic approximation, the stationary Schrödinger equation for the electrons reads

$$\hat{H}_{\text{el}}(\bar{\mathbf{R}})\Phi_v(\bar{\mathbf{r}}, \bar{\mathbf{R}}) = E_v(\bar{\mathbf{R}})\Phi_v(\bar{\mathbf{r}}, \bar{\mathbf{R}}) \quad (1)$$

with the electronic Hamiltonian

$$\begin{aligned} \hat{H}_{\text{el}} = & -\frac{1}{2} \sum_{i=1}^N \Delta_{\mathbf{r}_i} - \sum_{\alpha=1}^M \sum_{i=1}^N \frac{Z_\alpha}{|\mathbf{r}_i - \mathbf{R}_\alpha|} + \frac{1}{2} \sum_{i \neq j}^N \frac{1}{|\mathbf{r}_i - \mathbf{r}_j|} \\ & i,j = 1 \end{aligned} \quad (2)$$

Here, $\{\Phi_v(\bar{\mathbf{r}}; \bar{\mathbf{R}})\}$ is a set of adiabatic electronic wave functions, where $v = 0$ indicates the ground state and all $v > 0$ the excited states of the system.

2.1 | Effective Single-Particle Ground State Approaches

The electronic Schrödinger equation (Equation 1) is in practice still not solvable for many-body systems, due to the presence of the electron–electron interaction $\hat{V}_{\text{el-el}}$. The Green's function methods we discuss in this review aim at descriptions of single- or two-particle excited states. As most of the common formulations require information about the ground state electronic structure, we begin the discussion with effective single-particle methods for the ground state.

In the Hartree–Fock method [36], an ansatz is made for the many-electron wave function based on single-electron functions $\phi_i(\mathbf{r}_i)$, enforcing the antisymmetry with respect to particle exchange via the Slater determinant [37]:

$$\Phi^{\text{HF}}(\bar{\mathbf{r}}; \bar{\mathbf{R}}) = \frac{1}{\sqrt{N!}} \det \begin{pmatrix} \phi_1(\mathbf{r}_1) & \cdots & \phi_1(\mathbf{r}_N) \\ \phi_2(\mathbf{r}_1) & \cdots & \phi_2(\mathbf{r}_N) \\ \vdots & \ddots & \vdots \\ \phi_N(\mathbf{r}_1) & \cdots & \phi_N(\mathbf{r}_N) \end{pmatrix} \quad (3)$$

With the help of the variational principle, a set of equations to determine the single-particle functions can be derived:

$$\left\{ -\frac{\Delta_{\mathbf{r}}}{2} + v_{\text{ext}}(\mathbf{r}) + \int n(\mathbf{r}') v_C(\mathbf{r}, \mathbf{r}') d\mathbf{r}' \right\} \phi_j^{\text{HF}}(\mathbf{r}) \quad (4)$$

$$-\int n(\mathbf{r}, \mathbf{r}') v_C(\mathbf{r}, \mathbf{r}') \phi_j^{\text{HF}}(\mathbf{r}') d\mathbf{r}' = \epsilon_j^{\text{HF}} \phi_j^{\text{HF}}(\mathbf{r}) \quad (5)$$

with $v_C = |\mathbf{r} - \mathbf{r}'|^{-1}$. Here, we have also introduced the electronic densities

$$n(\mathbf{r}) = \sum_{i=1}^N \phi_i^*(\mathbf{r}) \phi_i(\mathbf{r}) \text{ and } n(\mathbf{r}, \mathbf{r}') = \sum_{i=1}^N \phi_i^*(\mathbf{r}) \phi_i(\mathbf{r}') \quad (6)$$

The first integral in Equation (5) corresponds to the classical Hartree integral [36] of the Coulomb interaction $v_H(\mathbf{r}) = \int n(\mathbf{r}') v_C(\mathbf{r}, \mathbf{r}') d\mathbf{r}'$, and the second integral defines the exchange potential operator $v_x(\mathbf{r}) = \int n(\mathbf{r}, \mathbf{r}') v_C(\mathbf{r}, \mathbf{r}') \dots d\mathbf{r}'$. The N -electron problem has thus been mapped on a set of effective single-particle problems with the Hartree–Fock potential

$$v_{\text{HF}}(\mathbf{r}) = v_{\text{ext}}(\mathbf{r}) + v_H(\mathbf{r}) + v_x(\mathbf{r}) \quad (7)$$

Hohenberg and Kohn [4] realized that one does not even need the full many-electron wave function to find the ground state of a many-electron system and that instead the electron density $n(\mathbf{r})$ alone is enough to determine the ground state. Within the Kohn–Sham framework of DFT, the density is again determined from another set of effective single-particle wave functions, which can be obtained as solutions to the Kohn–Sham equations [5]:

$$\left\{ -\frac{1}{2} \Delta + v_{\text{ext}}(\mathbf{r}) + v_H(\mathbf{r}) + v_{\text{xc}}[n](\mathbf{r}) \right\} \phi_i^{\text{KS}}(\mathbf{r}) = \epsilon_i^{\text{KS}} \phi_i^{\text{KS}}(\mathbf{r}) \quad (8)$$

with the effective Kohn–Sham Hamiltonian

$$\hat{H}_{\text{KS}} = -\frac{1}{2} \Delta + v_{\text{KS}}[n](\mathbf{r}) = -\frac{1}{2} \Delta + v_{\text{ext}}(\mathbf{r}) + v_H(\mathbf{r}) + v_{\text{xc}}[n](\mathbf{r}) \quad (9)$$

Despite their formal differences, we can write both HF and DFT in more general terms as mean-field (MF) single-particle methods with Hamiltonians

$$\hat{H}^{\text{MF}} = -\frac{\Delta}{2} + v_{\text{ext}} + v_H + v^{\text{MF}} = \hat{h} + v^{\text{MF}} \quad (10)$$

in which

$$v^{\text{MF}} = \begin{cases} v_x & \text{MF} = \text{HF} \\ v_{\text{xc}} & \text{MF} = \text{KS} \end{cases} \quad (11)$$

Both the Hartree–Fock method and Kohn–Sham DFT provide a framework to calculate the ground state of an interacting many-electron system. We note in passing that pure KS-DFT and HF can also be found as limiting cases within the generalized Kohn–Sham framework [38]. There are various ways to obtain information about excited states in these frameworks, for example, by time-dependent formulations (explicit or within linear response). Alternatively, one can consider electronic excitations as perturbations to the ground state and obtain again effective single- or two-particle formulations for the excitations and their energies within the framework of perturbation theory with many-body Green's functions.

2.2 | Single-Particle Excitations and the GW Approximation

Hedin derived a closed set of equations that define the single-particle Green's function $G_1(\mathbf{r}_1 t_1, \mathbf{r}_2 t_2)$ for an interacting set of electrons [39, 40]. The main idea, firstly introduced within the Dyson's equation of motion framework, is to truncate an infinite hierarchy of equations of motions for G_1 depending on higher-order Green's functions G_2, G_3, \dots by the introduction of the self-energy $\Sigma(\mathbf{r}_1 t_1, \mathbf{r}_2 t_2)$ which is an effective non-local, non-Hermitian potential, accounting for all many-body exchange and correlation terms that are beyond the scope of Hartree contributions. Hedin derived a self-consistent formulation of Dyson's equation of motion where distinct building blocks such as Green's function, screened Coulomb interaction, polarization, self-energy, and vertex correction interact self-consistently with each other [39, 40]. Hedin's equations can be simplified by the so-called *GW* approximation, in which the self-energy is written as $\Sigma = iG\omega$, and allows to derive a set of effective single-particle eigenvalue problems known as the *quasiparticle* (QP) equations

$$\begin{aligned} & \hat{H}^{\text{MF}} \phi_i^{\text{QP}}(\mathbf{r}) - v^{\text{MF}}(\mathbf{r}) \phi_i^{\text{QP}}(\mathbf{r}) \\ & + \int \Sigma(\mathbf{r}, \mathbf{r}', \epsilon_i^{\text{QP}}) \phi_i^{\text{QP}}(\mathbf{r}') d^3 r' = \epsilon_i^{\text{QP}} \phi_i^{\text{QP}}(\mathbf{r}) \end{aligned} \quad (12)$$

Typically, the QP wave functions $\phi_i^{\text{QP}}(\mathbf{r})$ are approximated by the mean-field wave functions $\phi_i^{\text{MF}}(\mathbf{r})$, which allows to write the QP energies as

$$\epsilon_i^{\text{QP}} = \epsilon_i^{\text{MF}} + \left\langle \phi_i^{\text{MF}} \left| \Sigma \left(\epsilon_i^{\text{QP}} \right) - v^{\text{MF}} \right| \phi_i^{\text{MF}} \right\rangle \quad (13)$$

The self-energy is calculated in frequency space as

$$\Sigma(\mathbf{r}, \mathbf{r}', \omega) = \frac{i}{2\pi} \int G(\mathbf{r}, \mathbf{r}', \omega + \omega') W(\mathbf{r}, \mathbf{r}', \omega') e^{i\omega' \eta} d\omega' \quad (14)$$

from the Green's function based on the mean-field solution

$$G(\mathbf{r}, \mathbf{r}', \omega) = \sum_m \frac{\phi_m^{\text{MF}}(\mathbf{r}) \phi_m^{\text{MF}*}(\mathbf{r}')}{\omega - \epsilon_m^{\text{MF}} - i\eta \text{sgn}(E_F - \epsilon_m^{\text{MF}})} \quad (15)$$

and the screened Coulomb interaction W in the random-phase approximation

$$W(\mathbf{r}, \mathbf{r}', \omega) = \int \epsilon^{-1}(\mathbf{r}, \mathbf{r}'', \omega) v_C(\mathbf{r}'', \mathbf{r}') d^3 r'' \quad (16)$$

Evaluating Equation (16) in turn requires the microscopic, frequency-dependent dielectric function given by

$$\epsilon(\mathbf{r}, \mathbf{r}', \omega) = \delta(\mathbf{r}, \mathbf{r}') - \int v_C(\mathbf{r}, \mathbf{r}'') \chi_0(\mathbf{r}'', \mathbf{r}', \omega) d\omega' \quad (17)$$

containing the irreducible polarizability χ_0 :

$$\chi_0(\mathbf{r}, \mathbf{r}', \omega) = \sum_v^{\text{occ}} \sum_c^{\text{unocc}} \left\{ \frac{\phi_v^{\text{MF}*}(\mathbf{r}) \phi_c^{\text{MF}}(\mathbf{r}) \phi_c^{\text{MF}*}(\mathbf{r}') \phi_v^{\text{MF}}(\mathbf{r}')}{\omega - (\epsilon_c^{\text{MF}} - \epsilon_v^{\text{MF}}) + i\eta} \right. \quad (18)$$

$$\left. - \frac{\phi_v^{\text{MF}}(\mathbf{r}) \phi_c^{\text{MF}*}(\mathbf{r}) \phi_c^{\text{MF}}(\mathbf{r}') \phi_v^{\text{MF}*}(\mathbf{r}')}{\omega + (\epsilon_c^{\text{MF}} - \epsilon_v^{\text{MF}}) - i\eta} \right\} \quad (19)$$

As the self-energy is energy-dependent, and thus depends on ϵ_i^{QP} , the solution of Equation (13) must be found self-consistently. From Equation (17) it is possible to split the self-energy $\Sigma = iGW$ into its bare exchange part

$$\begin{aligned} \Sigma^x(\mathbf{r}, \mathbf{r}') &= \frac{i}{2\pi} \int G(\mathbf{r}, \mathbf{r}' \omega + \omega') v_C(\mathbf{r}, \mathbf{r}') e^{i\omega' \eta} d\omega' \\ &= - \sum_v^{\text{occ}} \phi_v^{\text{MF}}(\mathbf{r}) \phi_v^{\text{MF}*}(\mathbf{r}') v_C(\mathbf{r}, \mathbf{r}') \end{aligned} \quad (20)$$

and the explicitly frequency-dependent correlation part

$$\Sigma^c(\mathbf{r}, \mathbf{r}', \omega) = \frac{i}{2\pi} \int G(\mathbf{r}, \mathbf{r}', \omega + \omega') (W(\mathbf{r}, \mathbf{r}', \omega') - v_C(\mathbf{r}, \mathbf{r}')) d\omega' \quad (21)$$

With $\omega_i = \epsilon_i^{\text{MF}} + \langle \phi_i^{\text{MF}} | \Sigma^x - v^{\text{MF}} | \phi_i^{\text{MF}} \rangle$ and $\langle \phi_i^{\text{MF}} | \Sigma^c(\omega) | \phi_i^{\text{MF}} \rangle = \Sigma_i^c(\omega)$, we can rewrite Equation (13) into the fixed-point problem

$$\omega - \omega_i = \Sigma_i^c(\omega) \quad (22)$$

Due to the pole structure of the self-energy, there are in general several solutions to Equation (22). In this situation, the spectral weight, defined as

$$Z(\omega) = \left(1 - \frac{d\Sigma^c(\omega)}{d\omega} \right)^{-1} \quad (23)$$

is used to identify the “true” QP energy by $Z(\omega) \approx 1$, or $|d\Sigma^c(\omega)/d\omega| \approx 0$.

In the above, when evaluating the self-energy, the MF eigenvalues and eigenfunctions are used to construct G and W , which is also known as an “one-shot” $G_0 W_0$ calculation. Alternatively, it is possible to use updated QP energies until eigenvalue self-consistency is reached ($\text{ev}GW$) [25, 41, 42].

2.3 | Coulomb Hole Plus Screened Exchange Approximation

As can be seen from the above, the frequency dependence of the self-energy gives rise to several computational intricacies. If one considers only the static case, in which $W(\mathbf{r}, \mathbf{r}', \omega = 0)$ throughout, one can split the self-energy differently. In analogy to the bare exchange term in HF or Σ^x , one can define a statically screened exchange (SEX) term as

$$\Sigma^{\text{SEX}}(\mathbf{r}, \mathbf{r}') = - \sum_v^{\text{occ}} \phi_v^{\text{MF}}(\mathbf{r}) \phi_v^{\text{MF}*}(\mathbf{r}') W(\mathbf{r}, \mathbf{r}', \omega = 0) \quad (24)$$

and a local-in-space static Coulomb hole (COH) term

$$\Sigma^{\text{COH}}(\mathbf{r}, \mathbf{r}') = \delta(\mathbf{r} - \mathbf{r}') [W(\mathbf{r}, \mathbf{r}', \omega = 0) - v_C(\mathbf{r}, \mathbf{r}')] \quad (25)$$

This COHSEX approach has been discussed in the literature as an alternative mean-field potential v^{MF} to use in Equation (10), yielding in some cases improved starting points for then dynamically screened GW calculations. It is mentioned here as it is also used in several approaches for environment embedding, as will be discussed in Section 3.

2.4 | Two-Particle Excitations and the Bethe-Salpeter Equation

The quasiparticle approach making use of the GW approximation is suitable for modeling single particle excitations such as the addition or removal of an electron to/from the system. However, charge-neutral excitations that involve excitonic effects (electron–hole pair interaction) are not accounted for, as they require a two-particle Green's function in the context of many-body Green's functions theory. The corresponding equation-of-motion can be expressed after some manipulation as a non-Hermitian eigenvalue problem known as *Bethe-Salpeter equation* (BSE)

$$\underline{\mathbf{H}}^{\text{BSE}} |\zeta_S\rangle = \Omega_S |\zeta_S\rangle \quad (26)$$

in which the electron–hole wave functions $|\zeta_S\rangle$ are typically expressed in basis of resonant and antiresonant products of single-particle functions (with c and v indices for unoccupied and occupied states, respectively)

$$\zeta_S(\mathbf{r}, \mathbf{r}') = A_{vc}^S \phi_c(\mathbf{r}) \phi_v^*(\mathbf{r}') + B_{vc}^S \phi_v(\mathbf{r}) \phi_c^*(\mathbf{r}') \quad (27)$$

With that, the BSE explicitly reads in matrix form

$$\begin{pmatrix} \underline{\mathbf{H}}^{\text{res}} & \underline{\mathbf{K}} \\ -\underline{\mathbf{K}} & -\underline{\mathbf{H}}^{\text{res}} \end{pmatrix} \begin{pmatrix} \mathbf{A}^S \\ \mathbf{B}^S \end{pmatrix} = \Omega_S \begin{pmatrix} \mathbf{A}^S \\ \mathbf{B}^S \end{pmatrix} \quad (28)$$

with elements

$$H_{vc,v'c'}^{\text{res}}(\omega) = D_{vc,v'c'} + K_{vc,v'c'}^x + K_{vc,v'c'}^d \quad (29)$$

$$K_{cv,v'c'}(\omega) = K_{cv,v'c'}^x + K_{cv,v'c'}^d \quad (30)$$

and

$$D_{vc,v'c'} = (\epsilon_c - \epsilon_v) \delta_{vv'} \delta_{cc'} \quad (31)$$

$$K_{vc,v'c'}^x = \int \phi_c^*(\mathbf{r}) \phi_v(\mathbf{r}) v_C(\mathbf{r}, \mathbf{r}') \phi_{c'}(\mathbf{r}') \phi_{v'}^*(\mathbf{r}') d^3 r d^3 r' \quad (32)$$

$$K_{vc,v'c'}^d = \int \phi_c^*(\mathbf{r}) \phi_{c'}(\mathbf{r}) \phi_v(\mathbf{r}') \phi_{v'}^*(\mathbf{r}') W(\mathbf{r}, \mathbf{r}', \omega = 0) d^3 r d^3 r' \quad (33)$$

For many systems, the off-diagonal blocks K in Equation (28) are small and can be neglected known as the Tamm–Danoff approximation (TDA). This makes the BSE matrix a Hermitian matrix. Furthermore, we can also ignore backward transitions which lead to:

$$\underline{\mathbf{H}}^{\text{res}} \mathbf{A}^{S,\text{TDA}} = \Omega_S^{\text{TDA}} \mathbf{A}^{S,\text{TDA}} \quad (34)$$

and the resulting electron–hole amplitude:

$$\zeta_S^{\text{TDA}}(\mathbf{r}, \mathbf{r}') = \sum_{vc} A_{vc}^{\text{TDA}} \phi_c(\mathbf{r}) \phi_v^*(\mathbf{r}') \quad (35)$$

We have suppressed the explicit spin variables so far. The spin structure of the BSE solutions depends on the spin-orbit coupling. If the ground state is a spin singlet state and spin-orbit coupling is small compared with the electron–hole coupling, the single particles can be classified as spin-up state or spin-down state. It can be shown that there are two distinct types of solutions to the BSE: spin-singlet and spin-triplet excitations. This allows in turn, to solve the BSE separately for the spin type of interest, with

$$H_{\text{singlet}}^{\text{BSE}} = D + K^d + 2K^x \quad (36)$$

$$H_{\text{triplet}}^{\text{BSE}} = D + K^d \quad (37)$$

respectively.

2.5 | Computational Aspects

All quantities involved in *GW*-BSE calculations are based on the mean-field single-electron wave functions ϕ_i^{MF} and energies ϵ_i^{MF} . Most implementations for isolated, molecular systems make use of localized basis functions, or atomic orbitals (AO), $\varphi_\alpha(\mathbf{r})$ and expansion coefficients c_α^i according to

$$\phi_i(\mathbf{r}) = \sum_{\alpha=1}^{N_b} c_\alpha^i \varphi_\alpha(\mathbf{r}) \quad (38)$$

Inserting this into Equation (10), multiplying from the left with $\varphi_\beta(\mathbf{r})$, and subsequent integration yields

$$\sum_{\alpha=1}^{N_b} \underbrace{\int \varphi_\beta(\mathbf{r}) \hat{H}_{\beta\alpha}^{\text{MF}} \varphi_\alpha(\mathbf{r}) d^3 r c_\alpha^i}_{F_{\beta\alpha}^{\text{MF}}} = \sum_{\alpha=1}^{N_b} \underbrace{\int \varphi_\beta(\mathbf{r}) \varphi_\alpha(\mathbf{r}) d^3 r c_\alpha^i \epsilon_i^{\text{MF}}}_{S_{\beta\alpha}} \quad (39)$$

with the integrals $F_{\beta\alpha}$ and $S_{\beta\alpha}$ defining the elements of the so called Fock matrix $\underline{\mathbf{F}}$ and overlap matrix $\underline{\mathbf{S}}$, respectively. The Fock matrix comprises terms from the one-electron contributions to $\hat{H}_{\beta\alpha}^{\text{MF}}$ (kinetic energy and external potential) also referred to as core Hamiltonian $\underline{\mathbf{h}}_{\text{core}}$, from the classical Hartree contribution $\underline{\mathbf{J}}$, explicit exchange $\underline{\mathbf{K}}$ in hybrid DFT or HF, and from the exchange-correlation potential $\underline{\mathbf{V}}_{\text{xc}}$ in DFT. Note that in general, the basis functions are normalized but not orthogonal to each other, and $\underline{\mathbf{S}} \neq \underline{\mathbf{I}}$. With this matrix notation, Equation (39) can be written as

$$\underline{\mathbf{F}}^{\text{MF}} \mathbf{c}^i = \epsilon_i^{\text{MF}} \underline{\mathbf{S}} \mathbf{c}^i \quad (40)$$

and the electron density can then be rewritten as

$$n(\mathbf{r}) = \sum_{i=1}^N |\phi_i(\mathbf{r})|^2 = \sum_{\alpha,\beta=1}^{N_b} D_{\alpha\beta} \varphi_\alpha(\mathbf{r}) \varphi_\beta(\mathbf{r}) \quad (41)$$

Here, we introduce the density matrix $\underline{\mathbf{D}}$ as

$$D_{\alpha\beta} = \sum_{i=1}^N c_\alpha^i c_\beta^i \quad (42)$$

A particularly important numerical step in *GW*-BSE calculations is the determination of 4-center repulsion integrals over the Gaussian-type orbitals (GTOs)

$$(\alpha\beta|\alpha'\beta') = \int \frac{\varphi_\alpha(\mathbf{r}) \varphi_\beta(\mathbf{r}) \varphi_{\alpha'}(\mathbf{r}') \varphi_{\beta'}(\mathbf{r}')}{|\mathbf{r}-\mathbf{r}'|} d^3 r d^3 r' \quad (43)$$

which are required for setting up the MF Hamiltonian as well as the self-energy. This step usually scales with N_b^4 (with N_b the number of basis functions). As one can see from Equation (43), GTOs occur as product functions $\varphi_\alpha(\mathbf{r}) \varphi_\beta(\mathbf{r})$, of which N_b^2 unique combinations exist. They can be approximated by a smaller auxiliary basis, ξ_μ , which contains only $N_{\text{aux}} = 3N_b$ to $5N_b$ functions instead. Rewriting the 4-center integrals as a combination of 3-center and 2-center repulsion integrals [43] reduces the scaling from N_b^4 to N_b^3 by:

$$(\alpha\beta|\alpha'\beta') \approx \sum_{\mu,\nu} (\alpha\beta|\mu)(\mu|\nu)^{-1}(\nu|\alpha'\beta') \quad (44)$$

where $(\mu|\nu)^{-1}$ is an element of the inverse of the 2-center repulsion matrix

$$(\mu|\nu) = \int \xi_\mu(\mathbf{r}) v_C(\mathbf{r}, \mathbf{r}') \xi_\nu(\mathbf{r}') d^3r d^3r' \quad (45)$$

and $(\alpha\beta|\mu)$ is an element of the 3-center repulsion tensor

$$(\alpha\beta|\mu) = \int \varphi_\alpha(\mathbf{r}) \varphi_\beta(\mathbf{r}) v_C(\mathbf{r}, \mathbf{r}') \xi_\mu(\mathbf{r}') d^3r d^3r' \quad (46)$$

The expression in Equation (44) appears formally as the insertion of a resolution-of-identity (RI) with metric $(\nu|\mu)^{-1}$.

Within the RI approximation, the elements of the QP Hamiltonian in the basis of KS states contain $\Sigma_{mn}(E) = \langle \phi_m^{\text{MF}} | \hat{\Sigma}(E) | \phi_n^{\text{MF}} \rangle$, which are determined as

$$\Sigma_{mn}(E) = \sum_{\mu,\nu} \sum_l I_\mu^{ml} I_\nu^{nl} \frac{i}{2\pi} \int \frac{e^{i\omega\theta} \epsilon_{\mu\nu}^{-1}(\omega)}{E + \omega - \varepsilon_l \pm i\eta} d\omega \quad (47)$$

where the factor with $\theta \rightarrow 0^+$ ensures convergence of the integral, and the imaginary perturbations $\pm \eta$ avoid singularities on the real axis, where the plus (minus) is taken when l is occupied (unoccupied). Further,

$$I_\mu^{ml} = \sum_v (\mu|v)^{-1/2} \sum_{\alpha,\beta} c_\alpha^m c_\beta^l (\alpha\beta|v) = \sum_v (\mu|v)^{-1/2} M_v^{ml} \quad (48)$$

and

$$\epsilon_{\mu\nu}(\omega) = \delta_{\mu\nu} - 2 \sum_m^{\text{occ}} \sum_l^{\text{unocc}} I_\mu^{ml} I_\nu^{ml} \left[\frac{1}{\omega - (\varepsilon_m - \varepsilon_l) + 2i\eta} \right] \quad (49)$$

$$- \frac{1}{\omega + (\varepsilon_m - \varepsilon_l) - 2i\eta} \quad (50)$$

is called the dielectric matrix (cf., Equation 17).

3 | Embedding Strategies for Many-Body Green's Function Methods

We discuss the challenges of using the *GW* and *BSE* methods to analyze complex molecular systems, which are made up of molecules with enough structural disorder to localize electronic states. Due to the high computational cost and $\mathcal{O}(N^4)$ scaling of these methods, it is impractical to apply them to large systems such as solid–liquid interfaces, molecules in solution, complex alloys, and nanostructures. As a solution, embedding strategies are considered as they offer a good balance between accuracy and computational cost for modeling large molecular systems. In these strategies, a specific part of the system (I) is treated with higher accuracy (the subsystem of interest), while the rest (II) is addressed with a lower accuracy method (the embedding region). In this review, the high-accuracy Many-Body Green's function method (*GW-BSE*) is discussed as the preferred method for studying electronically excited states, and its coupling with different methods used in the embedding region is explored.

In broad terms, two distinct embedding strategies can be employed. The idea behind the *subtractive* and *additive* embeddings [44] is depicted somewhat simplified in Figure 1. In a

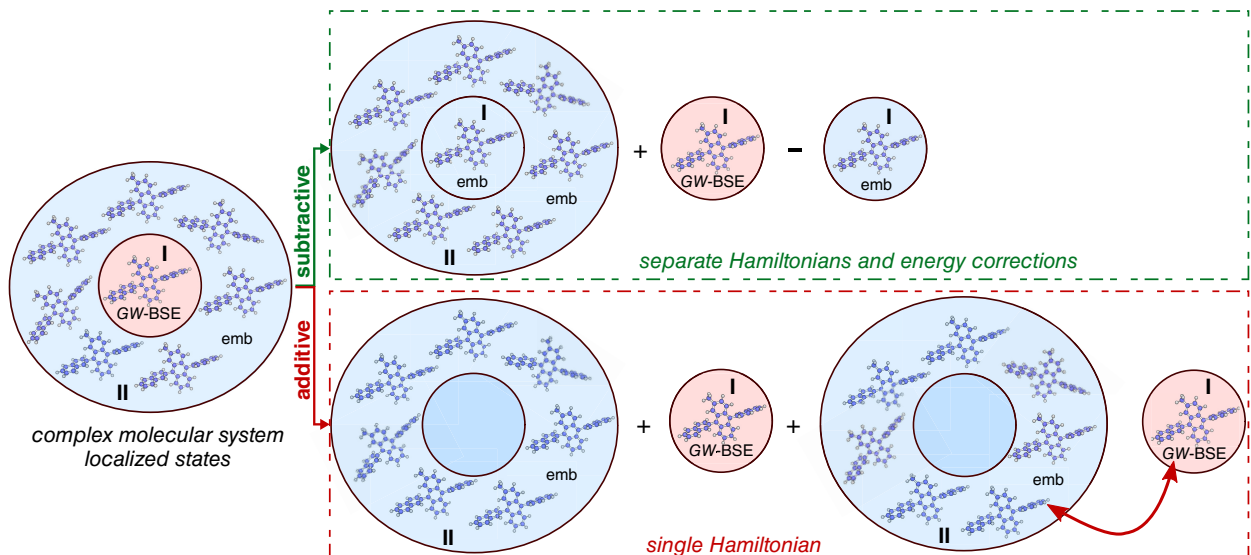


FIGURE 1 | Schematic representation of different QM/MM embedding schemes. The part figure (a) depicts the subtractive QM/MM scheme where the QM part is replaced by a classical counterpart, and the interaction between the inner and outer regions is treated purely classically. The QM region energy is shifted with the help of the classical contribution to avoid double counting. The part figure (b) shows the additive scheme where the MM and QM region energy are evaluated separately, with the interaction between the QM and MM part treated explicitly. Usually, the MM part enters the QM Hamiltonian as an external field, and the process is repeated until self-consistency is reached.

subtractive scheme, three separate calculations are performed: One *GW*-BSE calculation for the isolated subsystem I and calculations at the lower accuracy embedding method (emb), one for the entire system (subsystems I + II) and one for subsystem I. The total energy of the full system is then obtained as

$$E^{\text{sub}} = E_I^{\text{GW-BSE}} + E_{\text{I+II}}^{\text{emb}} - E_I^{\text{emb}} \quad (51)$$

The advantage of this approach is its simplicity: It automatically ensures that no interactions are double-counted. The embedded total energy of the full system is a simple sum, with the term $E_{\text{I+II}}^{\text{emb}} - E_I^{\text{emb}}$ considered as an energy correction.

On the other hand, the additive scheme total energy reads

$$E^{\text{add}} = E_I^{\text{GW-BSE}} + E_{\text{II}}^{\text{emb}} + V_{\text{I-II}}^{\text{GW-BSE-emb}} \quad (52)$$

where the *GW*-BSE system is embedded within the larger subsystem II and the interaction between the two regions is explicitly evaluated via the inclusion of the term $V_{\text{I-II}}^{\text{GW-BSE-emb}}$ in a coupled Hamiltonian and only a single calculation for the coupled system is required.

The above is only giving the broad strokes of embedding methods for many-body Green's functions as several important details remain vague: (i) what is the total energy of the *GW*-BSE system, (ii) what are suitable methods for the embedding, and (iii) how is the coupling term defined? The first question is straightforward to answer, considering

$$E_s^{\text{GW-BSE}} = \begin{cases} E_{\text{MF}} & \text{for } s = \text{ground state} \\ E_{\text{MF}} - \epsilon_s^{\text{QP}} & \text{for } s = \text{hole excitation} \\ E_{\text{MF}} + \epsilon_s^{\text{QP}} & \text{for } s = \text{electron excitation} \\ E_{\text{MF}} + \Omega_s^{\text{BSE}} & \text{for } s = \text{electron-hole excitation} \end{cases} \quad (53)$$

However, the state dependence of this energy highlights another complication, namely that unless the method chosen for the embedding is purely static, the individual terms in Equations (51) and (88) are all state-dependent, as well. As a consequence, embedded excitation energies need to be calculated as total energy difference, reminiscent of ΔSCF , that is,

$$\epsilon_s^{\text{QP,emb}} = E_{\text{gs}}^{\text{GW-BSE}} - E_s^{\text{GW-BSE}} \text{ for } s = \text{hole excitation} \quad (54)$$

$$\epsilon_s^{\text{QP,emb}} = E_s^{\text{GW-BSE}} - E_{\text{gs}}^{\text{GW-BSE}} \text{ for } s = \text{electron excitation} \quad (55)$$

$$\Omega_s^{\text{BSE,emb}} = E_s^{\text{GW-BSE}} - E_{\text{gs}}^{\text{GW-BSE}} \text{ for } s = \text{electron-hole excitation} \quad (56)$$

The above is, in principle at least, not unique to Green's function method approaches used as high-accuracy methods for subsystem I. We will see later that the state-dependence and total energy perspective can be partially circumvented making use of the dielectric screening intrinsically present in *GW*-BSE via the self-energy and the screened Coulomb interaction. Questions (ii) and (iii) will be addressed in the following sections where we will review some specific choices for embedding strategies in the

context of *GW*-BSE both from a methodological point of view and by showcasing application examples. We will differentiate embedding with other quantum-mechanical (QM/QM) methods and embedding with classical molecular mechanics (QM/MM) methods.

3.1 | *GW*-BSE-in-DFT Embedding

Here, we first consider the case in which the method for the embedding subsystem II is another mean-field quantum-mechanical method, specifically DFT, and focus on *GW*-BSE-in-DFT embedding methods. These approaches build on the fact that it is possible to partition the ground-state electronic density within DFT in an in-principle exact manner compared with a (sometimes fictitious) full treatment.

3.1.1 | Projection-Based Embedding

Projection-based embedding is a formally exact DFT-in-DFT embedding scheme, introduced by Manby et al. [45]. They proposed to partition the density of a full reference system $n(\mathbf{r})$ into the densities of two subsystems $n^{\text{I}}(\mathbf{r})$ and $n^{\text{II}}(\mathbf{r})$, such that $n(\mathbf{r}) = n^{\text{I}}(\mathbf{r}) + n^{\text{II}}(\mathbf{r})$. Then, one considers one of them (from now on $n^{\text{I}}(\mathbf{r})$) as active while the other (from now on $n^{\text{II}}(\mathbf{r})$) is regarded as an inactive embedding density. A set of effective Kohn–Sham equations for the (orbitals forming) active density embedded in the inactive density can be derived, and the resulting total energy of the embedded system can be made to agree exactly with the total energy of the full system. The first step of the algorithm is to perform a reference self-consistent DFT calculation on the complete system employing the full-molecule AO basis as described in Section 2.5. Then, a unitary transformation is used to transform the N occupied canonical molecular orbitals, $\phi_i(\mathbf{r})$ for $i = 1, \dots, N$, into localized orbitals, $\phi_i^{\text{LO}}(\mathbf{r})$. Note that this step leaves the total density of the system unchanged. Following this localization, an initial active density is constructed by selecting those localized orbitals with a significant Mulliken population $q_i^{\text{I}} > q_t$ on the atoms of the chosen subsystem I, yielding:

$$n^{\text{I}}(\mathbf{r}) = 2 \sum_{i=1}^N |\phi_i^{\text{LO}}(\mathbf{r})|^2 \quad (57)$$

$$q_i^{\text{I}} > q_t$$

The corresponding density of the inactive region is determined from this $n^{\text{I}}(\mathbf{r})$ as $n^{\text{II}}(\mathbf{r}) = n(\mathbf{r}) - n^{\text{I}}(\mathbf{r})$. With this initial partitioning of the total reference density into two subsystem densities, one now considers the active density as a variable in the subsystem I. A set of effective equations requires the addition of an embedding potential accounting for the electrostatic and exchange-correlation interactions with the electrons in subsystem II. At the same time, it must be ensured that the Pauli exclusion principle is not violated between the orbitals forming the densities of both subsystems. The main idea in projector-based embedding that fulfills both objectives is to raise the energies of orbitals associated with subsystem II to very high values during the calculation for subsystem I.

If we now consider $n^I(\mathbf{r})$ the initial density of the active region and denote the variable density as $\tilde{n}^I(\mathbf{r})$, the Fock matrix in the full-molecule AO basis for an embedded (I-in-II) calculation on the electrons in subsystem I is given by

$$\underline{\mathbf{F}}^{I\text{-in-}II} = \underline{\mathbf{h}}_{\text{core}}^{I\text{-in-}II} [n^I + n^{II}] + \underline{\mathbf{J}}[\tilde{n}^I] + \underline{\mathbf{K}}[\tilde{n}^I] + \underline{\mathbf{V}}_{\text{xc}}[\tilde{n}^I] \quad (58)$$

where $\underline{\mathbf{h}}_{\text{core}}^{I\text{-in-}II}$ is the embedded core Hamiltonian based on the partitioned initial densities n^I and n^{II} :

$$\underline{\mathbf{h}}_{\text{core}}^{I\text{-in-}II} [n^I + n^{II}] = \underline{\mathbf{h}}_{\text{core}} + \underline{\mathbf{J}}[n^I + n^{II}] - \underline{\mathbf{J}}[n^I] + \underline{\mathbf{K}}[n^I + n^{II}] - \underline{\mathbf{K}}[n^I] \quad (59)$$

$$+ \underline{\mathbf{V}}_{\text{xc}}[n^I + n^{II}] - \underline{\mathbf{V}}_{\text{xc}}[n^I] + \mu \underline{\mathbf{P}}_{II} \quad (60)$$

It contains the core Hamiltonian of the full system, the difference between the Hartree, exchange, and exchange-correlation terms for the full system and the initially chosen active subsystem, respectively, as well as a projection term $\mu \underline{\mathbf{P}}_{II}$ with the projection operator

$$\underline{\mathbf{P}}_{II} = \underline{\mathbf{S}} \underline{\mathbf{D}}^{II} \underline{\mathbf{S}} \quad (61)$$

based on the density matrix $\underline{\mathbf{D}}^{II}$ of the environment and the atomic orbital overlap matrix $\underline{\mathbf{S}}$ to ensure orthogonality between the occupied states of the environment and the rest of the active subsystem. The level-shift parameter μ is typically of the order of $10^5 - 10^6$ Hartree.

3.1.2 | Subsystem DFT

Compared with projection-based embedding, the subsystem-DFT (sDFT) approach does not start from a plain DFT reference calculation of the full system (see, e.g., [46, 47] for more details). Instead, the idea here is to perform Kohn-Sham-like calculations on fragments and then to determine the full-system density from the fragment densities. This way, the embedding region II can actually be split further into all molecular fragments. For the sake of presentation, we continue with the two region notation. Then, as in the projection-based embedding, the total electron density is given as $n(\mathbf{r}) = n^I(\mathbf{r}) + n^{II}(\mathbf{r})$, and each subsystem density is obtained from Kohn-Sham equations with constrained electron density (KSCE). To calculate the molecular orbitals of subsystem I in the frozen density n^{II} of subsystem II, these KSCE equations read [48–52]:

$$\left\{ -\frac{1}{2}\Delta + v_{\text{ext}}(\mathbf{r}) + v_H[n^I](\mathbf{r}) + v_{\text{xc}}[n^I](\mathbf{r}) + v_{\text{emb}}[n^I, n^{II}](\mathbf{r}) \right\} \phi_i^I(\mathbf{r}) = \epsilon_i^I \phi_i^I(\mathbf{r}) \quad (62)$$

where the embedding potential is

$$v_{\text{emb}}[n^I, n^{II}](\mathbf{r}) = v_H[n^{II}](\mathbf{r}) + v_{\text{xc}}[n^I + n^{II}](\mathbf{r}) - v_{\text{xc}}[n^I](\mathbf{r}) + \frac{\delta T_s^{\text{nadd}}[n^I, n^{II}]}{\delta n^I} \quad (63)$$

Here, the last term stems from the variation of the nonadditive kinetic energy $T_s[n^I + n^{II}] = T_s[n^I] + T_s[n^{II}] + T_s^{\text{nadd}}[n^I, n^{II}]$, and needs to be approximated in practical use. Note that in sDFT, the role of the subsystems (frozen vs. unfrozen density) must be

iterated until a convergence of the total energy of the full system is achieved.

3.2 | DFT-Embedded GW-BSE Calculations

Performing either projection-based embedding or sDFT calculation offers the advantage that the respective densities can be associated with the two (or more) subsystems and that the total density of the overall system is a sum of the subsystem densities. By construction, then also the occupied molecular orbitals of the subsystem of interest I are mostly localized in the respective spatial region. It is therefore possible, to limit the GW-BSE calculation to this “active” region only. For this, no changes in the formulation of the actual GW-BSE steps is required as the embedding potential is simply another external potential already included in the preceding DFT-in-DFT calculation. This implies, however, that all quantities involved use the embedded Kohn-Sham molecular orbitals and their energies as starting point. As these are changed with respect to the full reference case, one should not in general expect to obtain the same excitation energies from a GW-BSE calculation after subsystem-DFT as from a full GW-BSE calculation.

Examining the self-energy split into the exchange part Σ^X and correlation part Σ^C provides some insight into the qualitative differences. The expression of the exchange part in the molecular orbitals reads (c.f. Equation 21)

$$\Sigma^X(\mathbf{r}, \mathbf{r}') = -2 \sum_{i=1}^{N_{\text{occ}}} \phi_i^I(\mathbf{r}) \phi_i^I(\mathbf{r}') v_C(\mathbf{r}, \mathbf{r}') \quad (64)$$

and is therefore affected by two aspects: (i) summing over fewer occupied states in the DFT-embedded GW-BSE calculation and (ii) the changes in the molecular orbitals themselves. While Σ^X itself only depends on the occupied orbitals, it is important to realize that it enters the calculation of quasiparticle energies also of unoccupied states.

Performing a similar analysis for the frequency-dependent correlation part is more complicated. Recall first that Equation (21) gave

$$\Sigma^C(\mathbf{r}, \mathbf{r}', \omega) = \frac{i}{2\pi} \int G(\mathbf{r}, \mathbf{r}', \omega + \omega') (W(\mathbf{r}, \mathbf{r}', \omega') - v_C(\mathbf{r}, \mathbf{r}')) d\omega' \quad (65)$$

Here, the screened Coulomb interaction depends on the irreducible polarizability in the form (Equation 19)

$$\chi_0(\mathbf{r}, \mathbf{r}', \omega) = \sum_v^{\text{occ}} \sum_c^{\text{unocc}} \left\{ \frac{\phi_v^*(\mathbf{r}) \phi_c(\mathbf{r}) \phi_c^*(\mathbf{r}') \phi_v(\mathbf{r}')}{\omega - (\epsilon_c - \epsilon_v) + i\eta} - \frac{\phi_v(\mathbf{r}) \phi_c^*(\mathbf{r}) \phi_c(\mathbf{r}') \phi_v^*(\mathbf{r}')}{\omega + (\epsilon_c - \epsilon_v) - i\eta} \right\} \quad (66)$$

symbolically via

$$W = v_C + v_C \chi_0 W \quad (67)$$

In the exact reference calculation, the above is evaluated based on a full-DFT ground state. If one performs an embedded DFT calculation, the irreducible polarizability for subsystem I can be written with the respective labels as

$$\chi_0^I(\mathbf{r}, \mathbf{r}', \omega) = \sum_v^{\text{occ}} \sum_c^{\text{unocc}} \left\{ \frac{\phi_v^{I*}(\mathbf{r}) \phi_c^I(\mathbf{r}) \phi_c^{I*}(\mathbf{r}') \phi_v^I(\mathbf{r}')}{\omega - (\epsilon_c^I - \epsilon_v^I) + i\eta} - \frac{\phi_v^I(\mathbf{r}) \phi_c^{I*}(\mathbf{r}) \phi_c^I(\mathbf{r}') \phi_v^{I*}(\mathbf{r}')}{\omega + (\epsilon_c^I - \epsilon_v^I) - i\eta} \right\} \quad (68)$$

Subsystem embedding thus changes the polarizability. As the sum over occupied orbitals is limited to the active occupied orbitals, contributions to the screening from transitions that start from “originally” occupied orbitals of the embedding region are missing. This results in changes of the response even if the $\phi(\mathbf{r})$ and energies ϵ were unchanged. The lack of screening contributions from the now inactive region, generally translates into weaker contributions of Σ^c to the quasiparticle energies (in absolute values) in the DFT-embedded GW calculation compared with the full GW case. Even in weakly interacting, non-bonded molecular structures, for instance, where the orbitals themselves are only minimally affected by the embedding, one can expect to find the occupied (virtual) quasiparticle energies below (above) the ones from the full calculations. That means, in turn, that the HOMO-LUMO gap in subsystem- GW is also larger than the respective gap in full-system GW .

Examining now the electron–hole excitations on the level of the BSE, the reduction of the number of occupied orbitals limits the transitions used in the expansion of the two-particle wavefunctions to those starting from the active subsystem. Furthermore, different quasiparticle energies obtained at GW level directly affect the free transition term $D_{vc,v'c'}$ from Equation (31) in the BSE Hamiltonian. The exchange and direct (screened) terms of the electron–hole interaction kernel $K_{vc,v'c'}^x$ and $K_{vc,v'c'}^d$ are affected in similar ways from changes in the orbitals, energies, and screening as Σ^x and Σ^c , respectively. As a consequence of the reduced screening, a stronger electron–hole attraction can be expected compared with the full-system calculation. This stronger binding of electron and hole in turn compensates to some degree the increased quasiparticle gap entering the free transition term.

In [53, 54], Tölle et al. considered how additional screening effects from the environment can be incorporated in DFT-embedded GW -BSE calculations. Starting out from the screened Coulomb interaction of system I in the form of Equation (67):

$$W^{I-I} = v_C^{I-I} + v_C^{I-I} \chi_0^I W^{I-I} \quad (69)$$

where the superscript I-I indicates that the screened and bare Coulomb interaction only acts on orbitals in the region I. Including also the effects of the embedding subsystem II via its own irreducible polarizability χ_0^{II} , one obtains:

$$W^{I-I} = v_C^{I-I} + v_C^{I-I} \chi_0^I W^{I-I} + v_C^{I-II} \chi_0^{II} W^{I-I} \quad (70)$$

where

$$W^{II-I} = v_C^{II-I} + v_C^{II-I} \chi_0^I W^{I-I} + v_C^{II-II} \chi_0^{II} W^{II-I} \quad (71)$$

so that finally

$$W^{I-I} = (v_C^{I-I} + v_C^{I-II} \chi_0^{II} v_C^{II-I}) (1 + \chi_0^I W^{I-I}) + v_C^{I-II} \chi_0^{II} v_C^{II-I} \chi_0^{II} W^{II-I} \quad (72)$$

After further manipulations including the introduction of the interacting polarizability

$$\chi^I = \chi_0^I + \chi_0^I (v_C^{I-I} \chi^I + v_C^{I-II} \chi^{II}) \quad (73)$$

it is possible to rewrite

$$W^{I-I} = (v_C^{I-I} + v_C^{I-II} \chi^{II} v_C^{II-I}) (1 + \chi_0^I W^{I-I}) = \tilde{v}_C^{I-I} (1 + \chi_0^I W^{I-I}) \quad (74)$$

or equivalently

$$W^{I-I} = \tilde{v}_C^{I-I} + \tilde{v}_C^{I-I} \chi_0^I W^{I-I} \quad (75)$$

Note that if the system is composed of more than two subsystems, higher order terms (as many as the number of subsystems) need to be taken into account, and Equation (75) is then a one-body screening correction approximation. It includes a modified Coulomb interaction \tilde{v}_C^{I-I} , in which the term $v_{\text{reac}}^{I-I} = v_C^{I-II} \chi^{II} v_C^{II-I}$ can be interpreted as a reaction field, describing the fluctuation of a charge at a point \mathbf{r} due to a charge fluctuation at \mathbf{r}' both in subsystem I which is mediated by the polarization of subsystem II. With the help of the frequency-dependent dielectric function of subsystem I as

$$\epsilon^{I-I} = 1 - v_C^{I-I} \chi_0^I - v_{\text{reac}}^{I-I} \chi_0^I \quad (76)$$

one arrives at

$$W^{I-I} = \epsilon^{I-I^{-1}} [v_C^{I-I} + v_{\text{reac}}^{I-I}] \quad (77)$$

and easily sees that the reaction field appears both in the dielectric function and again in the modified Coulomb interaction.

Tölle et al. provided additional details about the implementation of the above for several subsystem fragments in different bases within the resolution-of-identity (RI) method in [53, 54], and we point the interested reader to the original work. The authors then reported the results of DFT-embedded GW -BSE calculations on an ammonia-benzene dimer, aqueous methylenecyclopropane, and a water-solvated adenine-thymine dimer. In Figure 2, we reprint from their work the dependence of the quasiparticle energy of the HOMO of ammonia in the ammonia-benzene dimer at different intermolecular separations (fig. 5 of [53]). One can clearly see that for both sDFT (here labeled as “Naddkin”) and projection-based-embedding (PbE), the plain embedded GW calculations without accounting for environment screening (blue open circles) from the benzene molecule yield lower quasiparticle energies than the supermolecular full system reference (open squares). The difference is largest for the closest dimer separation (around 0.2 eV) and becomes progressively smaller for larger distances. Note that Kohn–Sham energies for the HOMO already differ by about 0.05 eV in the respective ground state calculations for the shortest intermolecular separation (cf., fig. 4 of [53]). The inclusion of the environment screening here from the single

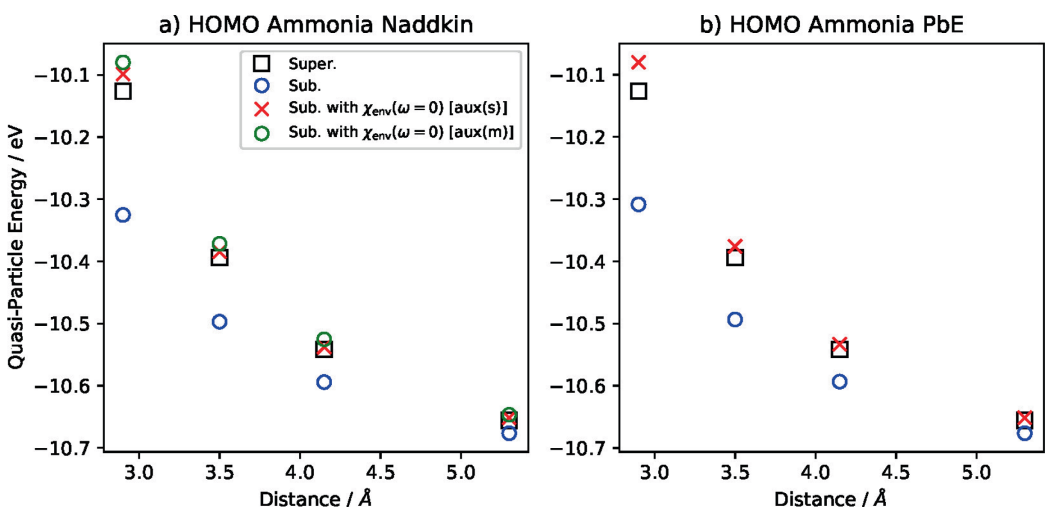


FIGURE 2 | Quasi-particle energy of the HOMO located on ammonia in an ammonia-benzene dimer with varying separation (see inset) using nonadditive kinetic (Naddkin) (a) or projection-based embedding (PbE) (b) [G_0W_0 @BLYP, def2-TZVP; aux(m), subsystem-only auxiliary basis; aux(s), supermolecular auxiliary basis].

benzene molecule (red crosses) brings the quasiparticle energies in very close agreement with the full calculations. The authors observed similar behavior for the quasiparticle energies of methylenecyclopropane with a variable number of water molecules as solvent and in water-solvated adenine-thymine dimers.

The authors also pointed out the importance of including the environment correction in both steps of the *GW*-BSE procedure when interested in electron–hole excitations. The screening enters both the calculation of the quasiparticle energies (and with that the free transition part of the BSE) and the electron–hole interaction kernel. The individual effects can be distinguished from the data shown in Figure 3 for solvated MCP. Without environment screening, the excitations are found at higher energies in the subsystem calculation as compared with the full reference. This is a combination of too large quasiparticle gap and too strong electron–hole interaction when the environment screening is not accounted for. One can see that when environment screening is included on *GW* level only the BSE energies are obtained several 0.1 eV below the reference—the free transition part is almost correct, so the deviation can be attributed to too strong electron–hole interaction. Only when the latter is also additionally screened, a very good agreement with the full system reference can be observed.

Overall, it could be demonstrated successfully that DFT-embedded *GW*-BSE calculations yield good agreement with full supermolecular *GW*-BSE calculations if even approximately, environment effects are taken into account. The downside of this approach is mainly its still significant computational cost when applied to large-scale systems with large molecules in active and inactive regions.

3.3 | *GW*-BSE-in-MM Embedding

Excited states in complex molecular systems are in general multi-scale, in the sense that intrinsic quantum-mechanical properties

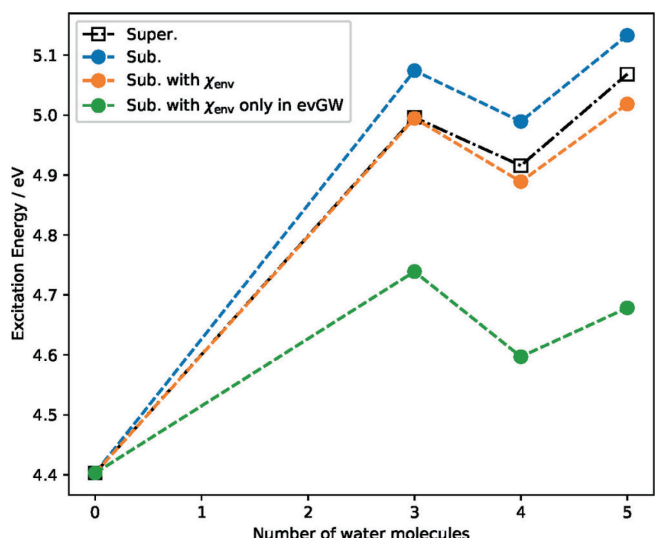


FIGURE 3 | BSE energies obtained from supermolecular and embedded evGW@PBE0-BSE(TDA) calculations for aqueous MCP. Reprinted (adapted) with permission from Journal of Chemical Theory and Computation 2021;17(4):2186–2199. Copyright 2021 American Chemical Society.

of the basic units, that is, isolated molecules, and the local and global morphology of the large-scale molecular system are intertwined. At this scale, the use of *GW*-BSE-in-DFT embedding as sketched in the previous section can be computationally extremely demanding, if not prohibitive. Similar notions also apply to other quantum-quantum embedding strategies [30, 31, 33].

A way to reduce such overly costly computations is to employ a classical (electrostatic) method for the embedding region, including, that is, approaches in which the environment of an electronically active region is replaced by a polarizable continuum [33, 34, 55, 56], or when it is represented by a classical, molecular mechanics parametrization (MM) [32, 57]. The *GW*-BSE formalism allows for different approaches to include such classical environmental polarizabilities. The one that we will

review first is conceptionally very similar to the *GW*-BSE-in-DFT embedding, in the sense that the environment response is directly included in the calculation of the screened Coulomb interaction W both in the *GW* and the BSE stages of the calculations. Later, we will also discuss alternative subtractive and additive quantum-classical approaches, which use total energies of coupled systems as introduced earlier rather than modifying the screened Coulomb interaction directly.

3.3.1 | Classical Environment Polarizability in W

While we present the idea of including a classical environment polarizability in the calculation of the screened Coulomb interaction of subsystem I after the *GW*-BSE-in-DFT embedding, these methods have been developed historically in different order. For the sake of presentation, we pick up from the definition of the modified Coulomb interaction in Equation (74) in *GW*-BSE-in-DFT embedding, which now in real-space form including the explicit dependence on the frequency ω reads

$$\tilde{v}_C^{I-I}(\mathbf{r}, \mathbf{r}', \omega) = v_C^{I-I}(\mathbf{r}, \mathbf{r}') + \int v_C^{I-II}(\mathbf{r}', \mathbf{r}_{II}) \chi^{II}(\mathbf{r}_{II}, \mathbf{r}'_{II}, \omega) v_C^{III}(\mathbf{r}'_{II}, \mathbf{r}) d\mathbf{r}_{II} d\mathbf{r}'_{II} \quad (78)$$

The integral on the right-hand side is the already introduced reaction field or reaction potential

$$v_{\text{reac}}^{II}(\mathbf{r}, \mathbf{r}', \omega) = \int v_C^{I-II}(\mathbf{r}', \mathbf{r}_{II}) \chi^{II}(\mathbf{r}_{II}, \mathbf{r}'_{II}, \omega) v_C^{II-I}(\mathbf{r}'_{II}, \mathbf{r}) d\mathbf{r}_{II} d\mathbf{r}'_{II} \quad (79)$$

The decisive step is now to introduce here a classical model of the polarizability of subsystem II, that is, $\chi^{II} \rightarrow \chi^{\text{MM}}$.

Essentially, a classical approximation to the environment polarizability only differs by the adoption of a specific model for χ^{MM} in place of the explicitly QM variant used in χ^{II} . There are, however, a few noteworthy aspects to this:

- i. There is not a single “one-size-fits-all” MM model for the environment polarizability, including continuum models (polarizable continuum model) as well as atomistic models of varying sophistication (Drude model [58, 59], charge equilibration [60, 61], distributed polarizabilities in Applequist [62], or Thole [63, 64] form).
- ii. Classical models need to be parametrized, in the simplest case (polarizable continuum model) with a macroscopic dielectric constant ϵ_r or with various element or atom-specific quantities (Drude, Thole, and charge equilibration).
- iii. Most if not all classical models cannot be cast in an explicit form $\chi^{\text{MM}}(\mathbf{r}_{II}, \mathbf{r}'_{II})$ that allows a straightforward evaluation of Equation (79).
- iv. Most if not all classical models only provide static polarizability in the zero-frequency limit ($\omega \rightarrow 0$) instead of full dynamic polarizability.

Trying to address the details and the respective strengths and weaknesses of the different classical polarization models and with that the steps required in their parametrization according

to points (i) and (ii) exceeds the scope of this review and we point the reader to the original literature, instead. We will focus on general remarks to points (iii) and (iv), which are to a large extent agnostic to the specifics of the MM models used. Duchemin, Jacquemin, and Blase [55] proposed to not calculate the real-space form of the reaction field, $v_{\text{reac}}^{II}(\mathbf{r}, \mathbf{r}', \omega)$, as in Equation (79) but instead exploit the resolution-of-identity (RI) method. Recall that in Equation (45), auxiliary basis functions ξ_μ were used to calculate two-center Coulomb repulsion integrals

$$\langle \mu | \nu \rangle = \int \xi_\mu(\mathbf{r}) v_C^{I-I}(\mathbf{r}, \mathbf{r}') \xi_\nu(\mathbf{r}') d\mathbf{r} d\mathbf{r}' \quad (80)$$

to be later used to calculate approximated four-center Coulomb integrals needed in the *GW*-BSE implementation. Herein, one ‘simply’ replaces $v_C^{I-I}(\mathbf{r}, \mathbf{r}') \rightarrow \tilde{v}_C^{II}(\mathbf{r}, \mathbf{r}')$, such that one has to additionally determine:

$$\langle \mu | \nu \rangle_{\text{reac}} = \int \xi_\mu(\mathbf{r}) v_{\text{reac}}^{II}(\mathbf{r}, \mathbf{r}') \xi_\nu(\mathbf{r}') d\mathbf{r} d\mathbf{r}' \quad (81)$$

Note that both functions ξ_μ and ξ_ν are auxiliary functions in the QM region (subsystem I). These integrals can be computed by considering the basis function ξ_μ as a charge distribution that polarizes the embedding region according to the adopted MM model. Then, the action of this response field on the basis function ξ_ν is calculated.

In the above, we have already conveniently ignored the frequency dependence, implying the use of the static limit, as was also done in *GW*-BSE-in-DFT embedding, for the whole frequency range. As an alternative, it was suggested also in [55] to use the COHSEX approximation (cf., Equations 24 and 25) to determine state-specific correction terms to the quasiparticle energies of an isolated system in a vacuum, ϵ_i^{QP} , as in

$$\epsilon_i^{\text{QP}, \Delta \text{COHSEX}} = \epsilon_i^{\text{QP}} + \left(\epsilon_i^{\text{COHSEX,emb}} - \epsilon_i^{\text{COHSEX}} \right) \quad (82)$$

As an example, the authors studied solvatochromic shifts of the first ionization potential (HOMO energy) for the four nucleobases adenine, cytosine, thymine, and uracil upon embedding in water represented by a polarizable continuum model. They pointed out the importance of carefully choosing the appropriate value of the dielectric constant for the embedding region, corresponding to fast and slow screening processes. The high dielectric constant of water ($\epsilon_r = [78.35]$) results as a combination of relaxation processes of electronic (fast) and nuclear (slow) degrees of freedom. The authors argue that while for the ground state, screening from both is appropriate, only the fast, electronic, processes can react to the excitation (ionization) process, and therefore one should use the *optical* dielectric constant $\epsilon_\infty = [1.78]$ in the embedded calculation, yielding in the end to an additional contribution to the solvatochromic shift: first, the ground-state is calculated based on DFT with PCM using the high ϵ_r , then a *GW* embedding calculation is performed starting from the molecular orbitals of this ϵ_r -embedded ground state, however using ϵ_∞ in the reaction field calculation. In Table 1, we reprint the results from this so-called non-equilibrium approach as reported in [55],

obtained with the direct use of the static approximation in the determination of the embedded quasiparticle calculations (here labeled ΔGW) and the $\Delta COHSEX$ variants, respectively. One can see that both approaches give very similar shifts in the non-equilibrium calculation with deviations < 0.05 eV. In an equilibrium calculation, that is, if ϵ_r is also used in the embedded GW step, the overall shifts are larger (due to the much larger polarization effect) as are the differences between ΔGW and $\Delta COHSEX$.

As a side note, we emphasize that the choice between this non-equilibrium vs. equilibrium scenario may depend on the type of excitation and the physical process of interest. Polarity-sensitive dyes, for instance, exhibit strong Stokes shifts of the optical emission energy with respect to the absorption energy in strongly polar solvents such as water. Here, however, nuclear relaxation by far dominates the effects of electronic degrees of freedom. Baral et al. [65] studied such nuclear relaxation effects for prodan also with coupled classical Molecular Dynamics- GW -BSE calculations (MM/ GW -BSE), in which no electronic polarization from the embedding region was taken into account, but only electrostatic background from the reorienting solvent molecules. As shown in Figure 4, this allows us to capture the nuclear relaxation on ps timescale and calculated Stokes shifts in good agreement with the experiment. We will revisit such

TABLE 1 | Solvatochromic shifts (in eV) of the first ionization potential of four nucleobases upon solvation in water represented by a PCM, as obtained by using the static approximation for χ^{MM} directly in the GW calculation (ΔGW) and by the $\Delta COHSEX$ approach.

	Adenine	Cytosine	Thymine	Uracil
Non-equilibrium				
ΔGW	0.60	0.67	0.95	1.05
$\Delta COHSEX$	0.64	0.70	0.99	1.07
Equilibrium				
ΔGW	1.51	1.67	1.92	1.96
$\Delta COHSEX$	1.64	1.75	2.03	2.15

Note: All data from [55].

external coupling between GW -BSE and MM regions in the following section.

What the previous example highlights is that excitation energies, no matter if charged or neutral, can also be affected by electrostatic effects from the environment that are not merely arising from polarization. Non-symmetrical structural details, for instance, combined with non-negligible electrostatic moments can cause additional shifts of excitation energies with respect to vacuum. Such situations are typically also present in low-dimensional systems, such as surfaces of molecular crystals. Li et al. [57] have extended the approach based on Equation (81) to study charged excitations at the (001) surface of a pentacene crystal. In particular, they used the charge response model by Tsiper and Soos to model the polarization effects [66] and combined it with long-range static embedding effects in the low-dimensional environment [67] to account for crystal field effects. Figure 5 shows how the inclusion of different environmental effects affects the calculated ionization potential and electron affinities at the surface. It is very obvious that polarization effects massively reduce the GW gap compared with the gas phase calculation (which agrees favorably with experimental results for gas phase ionization energies). From a purely electrostatic perspective, the excited electron and hole get screened, or energetically stabilized, in the same way, meaning that the ionization potential lowers and the electron affinity increases. Additional inclusion of the crystal field affects both excitation energies in the same direction, that is, the absolute energies are shifted, but their energy difference is more or less constant.

3.3.2 | External QM/MM

The methods presented in Section 3.3.1 provide ways to include screening effects from a classical environment into GW -BSE calculations utilizing additional terms in the screened Coulomb interaction W . In contrast to this *internal* inclusion of screening, alternative approaches focus on accounting for these effects with what we from now on refer to as *external* QM/MM. As the name suggests, the calculations for the QM and classical MM regions of such approaches are more separated than, for example, by evaluating the effects on an environment reaction field via Equation (81). Instead, the two regions are coupled based solely

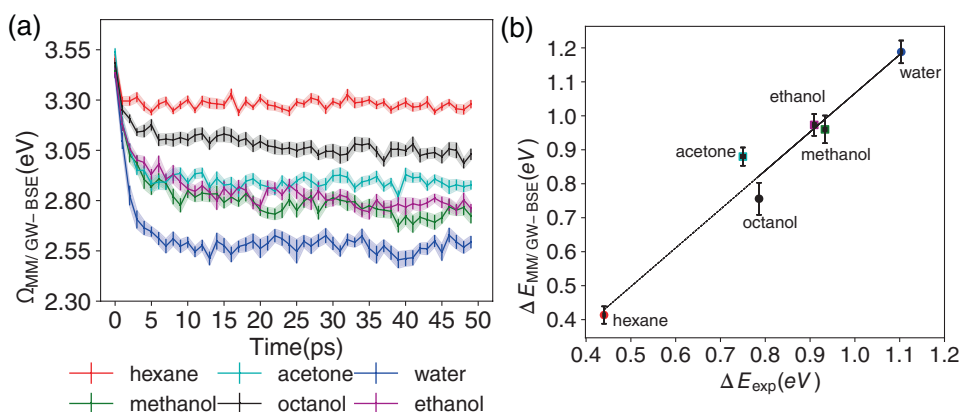


FIGURE 4 | (a) Time-dependent emission energy of prodan in different solvents and (b) final Stokes shifts as obtained from MM/ GW -BSE calculations from [65]. Reprinted (adapted) with permission from Journal of Physical Chemistry B 2020;124(13):2643–2265. Copyright 2020 American Chemical Society.

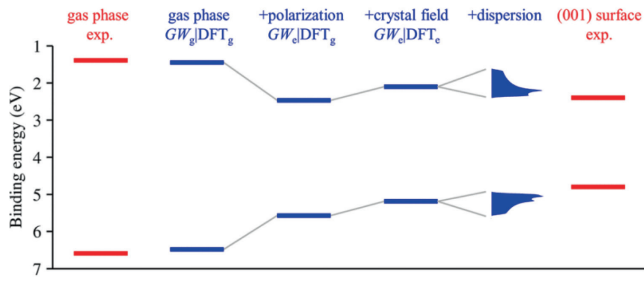


FIGURE 5 | Evolution of Ionization Potential and Electron Affinity from the gas phase to crystal surfaces for a pentacene crystal. Calculation results from [57] include different contributions from intermolecular interactions (polarization, crystal field, band dispersion) to the final excitation energies at the crystal surface. Reprinted (adapted) with permission from Physical Review B 2018;97:035108.

on electrostatic interactions. A typical workflow of such an external GW -BSE/MM calculation is shown in Figure 6. The four method ingredients are the classical microelectrostatics model, the DFT calculation for the ground state, as well as the GW and Bethe–Salpeter equation steps, respectively. The classical, polarizable environment in the MM region enters the GW -BSE workflow merely as a specific external potential on the level of the reference ground state calculation: the first element of the classical model is a set of static atomic multipoles that create a local electric field which polarizes the electronic density of the QM region. The second element is the addition of polarizable distributed atomic multipoles for molecules in the MM region (as mentioned in the Section 3.3.1). Combined with the static moments, the overall effect of polarization is a self-consistent reaction field *inside* the QM region. In the specific formulation of the *Thole model*, static atomic multipole moments [63, 64] are indicated as Q_t^m , where t is the multipole rank and m the associated atom in the molecule M . The interactions between the multipoles moments Q_t^m and $Q_u^{m'}$ are described by the tensor $T_{tu}^{mm'}$. To account for polarization, a polarizability $\alpha_{tu}^{mm'}$ is assigned to each atom. Interaction with the field generated by moments u on a different atom m' creates induced moments ΔQ_t^m . Consider now the splitting of a purely classical (MM) system S in state s into two regions \mathcal{R} and \mathcal{R}' with $S = \mathcal{R} \cup \mathcal{R}'$. Molecules in region \mathcal{R} (\mathcal{R}') are indicated by M (M'), and atoms in molecule M (M') by m (m'). The total classical energy of the system is then given by

$$E_{\text{class}}^{(s)}(S) = E^{(s)}(\mathcal{R}) + E^{(s)}(\mathcal{R}') + E^{(s)}(\mathcal{R}, \mathcal{R}') \quad (83)$$

where

$$E^{(s)}(\mathcal{R}) = \frac{1}{2} \sum_{M \in \mathcal{R}} \sum_{M' \in \mathcal{R}} E_{MM'}^{(s)} + \frac{1}{2} \sum_{M \in \mathcal{R}} E_M^{(s)} \quad (84)$$

$M' \neq M$

$$E^{(s)}(\mathcal{R}, \mathcal{R}') = \sum_{M \in \mathcal{R}} \sum_{M' \in \mathcal{R}'} E_{MM'}^{(s)} \quad (85)$$

with

$$E_{MM'}^{(s)} = \sum_{m \in M} \sum_{m' \in M'} \sum_{tu} \left(Q_t^{m(s)} + \Delta Q_t^{m(s)} \right) \times T_{tu}^{mm'} \left(Q_u^{m'(s)} + \Delta Q_u^{m'(s)} \right) \quad (86)$$

and

$$E_M^{(s)} = \sum_{m \in M} \sum_{m' \in M} \sum_{tu} \Delta Q_t^{m(s)} (\alpha^{-1})_{tu(s)}^{mm'} \Delta Q_u^{m'(s)} \quad (87)$$

$m' \neq m$

Equation (83) needs to be minimized with respect to the induced moments ΔQ_t^m . Note that other classical environment models differ mainly by the specific expressions used for Equations (86) and (87).

In a QM/MM setup, the total energy, cf. also Equation (52), is given as the sum of QM, MM, and QM/MM coupling terms:

$$E_{\text{QM/MM}}^{\text{add}} = E_1^{\text{QM}} + E_2^{\text{MM}} + V_{12}^{\text{QM/MM}} \quad (88)$$

Here, the two regions are explicitly coupled via the term $V_{12}^{\text{QM/MM}}$, that is, via electrostatic interactions between the two subsystems. These are accounted for by adding the external potential of the multipoles in the MM region to the QM Hamiltonian as one-electron operators during the computation of the electronic wave function. Vice-versa, the MM region is polarized by the explicit electrostatic field from the QM density. Specifically in GW -BSE, there are several options for this density, depending on the type of excitation (s). If s is a quasiparticle excitation, we define

$$n_{\text{QP}}^{(s)}(\mathbf{r}) = n_{\text{DFT}}(\mathbf{r}) + f_s |\phi_s^{\text{QP}}(\mathbf{r})|^2 \quad (89)$$

with $f_s = -1$ for occupied and $f_s = +1$ for unoccupied QPs. If s is an electron–hole excitation, its total density is evaluated as

$$n^{(s)}(\mathbf{r}) = n_{\text{DFT}}(\mathbf{r}) + n_e^{(s)}(\mathbf{r}) - n_h^{(s)}(\mathbf{r}) \quad (90)$$

Here the electron (hole) contribution of the exciton to the density is computed by integrating the squared excited-state wavefunction ζ_S with respect to the hole (electron) coordinates, that is,

$$\rho_e^{(s)}(\mathbf{r}) = \rho_e^{(s)}(\mathbf{r}_e) = \int d\mathbf{r}_h |\zeta_S(\mathbf{r}_e, \mathbf{r}_h)|^2 \quad (91)$$

$$\rho_h^{(s)}(\mathbf{r}) = \rho_h^{(s)}(\mathbf{r}_h) = \int d\mathbf{r}_e |\zeta_S(\mathbf{r}_e, \mathbf{r}_h)|^2 \quad (92)$$

The inclusion of a polarizable MM region requires a self-consistent procedure to evaluate the total QM/MM energy of a system in a given state s . At a single step p within this self-consistent procedure, first a QM level calculation (DFT for the ground state $s = g$, DFT + GW -BSE for electron–hole excited $s = x$ states) is performed in the electric field generated by the total moments in the MM region. The total energy of the QM region in state s is then given by Equation (53), and excitation energies are obtained from it and the energy of the classical region via “ Δ -QM/MM-SCF” formulations as total energy differences according to Equation (56). In Figure 7 this is indicated by the three different “routes” that the calculation

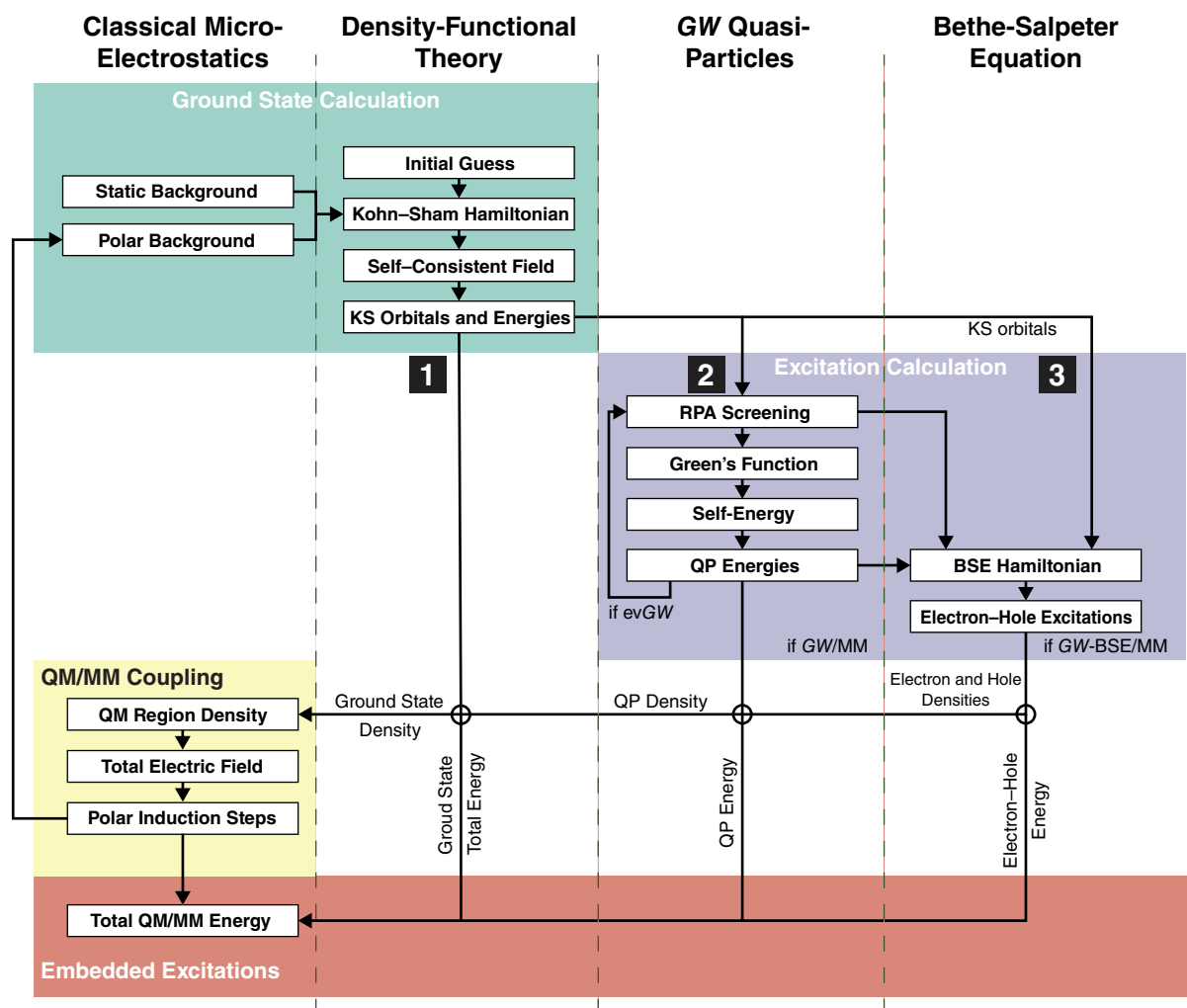


FIGURE 6 | Example of a typical workflow for externally embedded GW -BSE calculations combining classical microelectrostatics models with DFT and GW -BSE calculations in a QM/MM scheme. Three different routes to converged total energies are indicated: 1—ground state DFT/MM; 2—quasiparticle GW /MM; 3—electron-hole GW -BSE/MM.

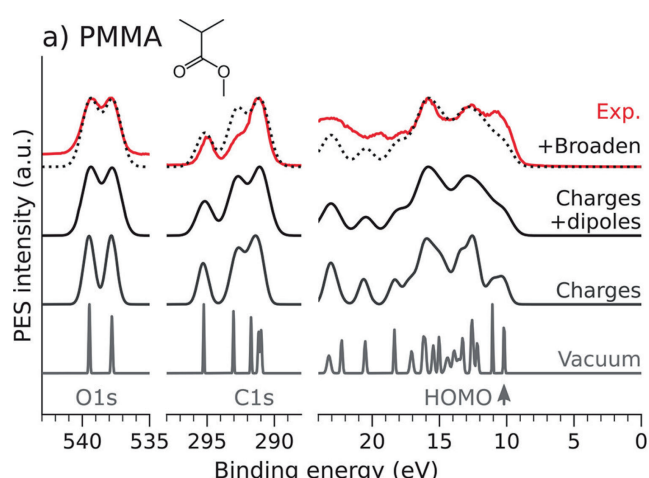


FIGURE 7 | Experimental and calculated photoelectron spectra for the O 1s, C 1s, and valence regions of amorphous polymethyl methacrylate (PMMA) [68]. Reprinted (adapted) with permission from Journal of Physical Chemistry Letters 2024;15(3):834–839. Copyright 2024 American Chemical Society.

can take through the algorithm: Route 1 corresponds to the reference ground state calculation in which the MM region has responded to the plain DFT density of the QM region; in route 2 the external polar field the MM enacts on the QM region is determined as a response from the quasiparticle density Equation (90) (GW /MM); and route 3 is used to get the total QM/MM energy in which the density in the QM region is determined according to Equation (92).

As a first example of an application of a variant of such a GW /MM embedding scheme, Galleni et al. [68] studied the peak broadening of photoemission spectra in amorphous polymers. Figure 7 shows as an example the obtained core level and valence region photoelectron spectra of polymethyl methacrylate (PMMA), where the data shown as “charges” correspond roughly speaking to a GW /MM calculation with no polarization in the MM region, while “charges + dipoles” include polarization effects. One can clearly see that intrinsic local inhomogeneities in the electrostatic environment induce a broadening of 0.2–0.7 eV in the binding energies of both core and semivalence electrons.

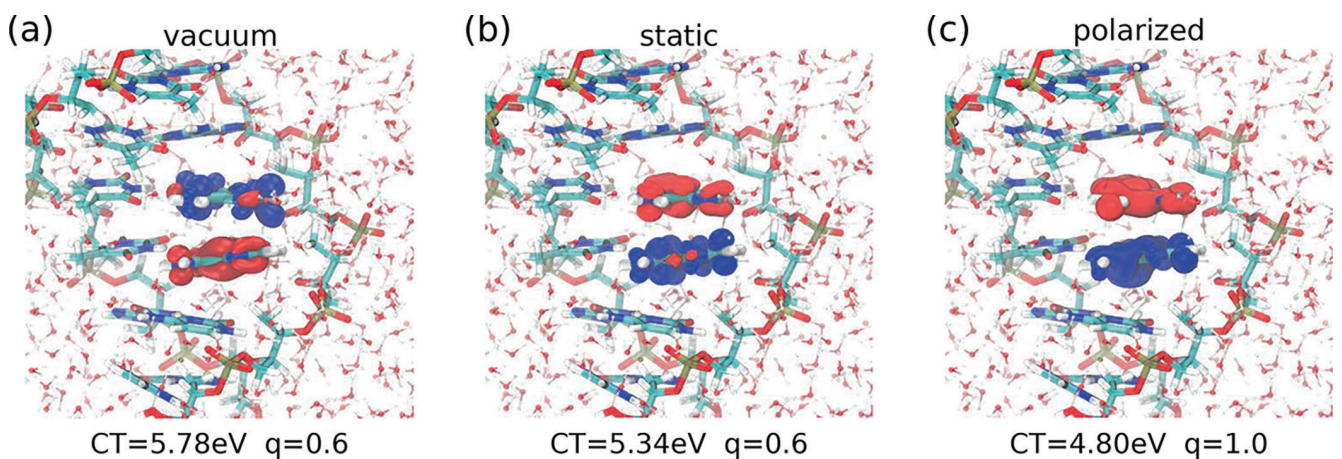


FIGURE 8 | Effect of polarization on charge-transfer excitons in solvated DNA from different *GW*-BSE calculations: (a) a single DNA base pair in vacuum, (b) the same base pair in an environment that is not polarizable, (c) the same base pair in a polarizable environment. Reprinted with permission from Journal of Chemical Theory and Computation 2018;14(12):6253. Copyright 2018 American Chemical Society.

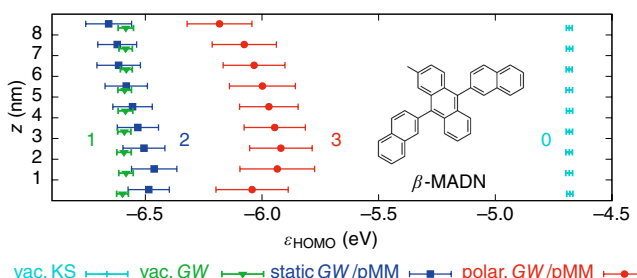


FIGURE 9 | Layer-resolved energy levels of a thin film consisting of 1000 β -MADN (see inset) molecules obtained at different levels of theory: Vacuum KS, vacuum *GW*, static, and polarizable *GW*+MM-in-MM including long-range effects with periodic embedding (labeled pMM), taken from [72]. The error bars correspond to the range of ± 1 SD. Reprinted (adapted) with permission from Physical Review B 2020;101:035403. Copyright 2020 American Physical Society.

Figure 8 shows in steps the effects of embedding of electron-hole excitations in *GW*-BSE/MM on the charge-transfer type excitations between two adenine base pairs in solvated double-stranded DNA. The progression from a *GW*-BSE calculation in vacuum, via a *GW*-BSE/MM with a non-polarizable environment, to *GW*-BSE/MM with a polarizable environment shows not only that the charge-transfer excitation energy is affected but also that the nature of the electronic excitation is also sensitive to effects from the complex environment. Here, for instance, the amount of transferred charge changes from a partial charge transfer of 0.6 e to an integer charge transfer of 1 e. It is also clear that this is an effect of polarization, as integer transfer is not observed with a static MM environment in Figure 8b. This is not only a consequence of the converged *GW*-BSE/MM calculation having different weights for the respective transitions between occupied and unoccupied single-electron states in Equation (27). Additionally, the single-particle functions themselves are affected by the inclusion of the contribution of polarized electrostatic moments in the external potential of the underlying ground-state calculation.

A notorious problem for the external *GW*-BSE/MM approaches with polarization is related to the self-consistency procedure in the quantum-classical iterations cycle. Evaluation of the QM

density as in Equation (90) or Equation (92) (and the respective energies) depending on the calculation route can be tricky as electronic energy levels can swap between iterations. Following the “correct” state is not always trivial, especially if polarization effects cause significant changes to the nature of the excitation, as they do in the example of Figure 8. Issues like these are well-known also for instance in geometry optimizations in excited states.

3.3.3 | Subtractive (MM-in-MM) Embedding

As attractive and powerful the embedding approaches presented in Sections 3.2 and 3.3 are, the calculations are, in general, still computationally demanding if applied to complex molecular systems. In some situations, it can be attractive to use a subtractive embedding scheme as mentioned in Section 3. Instead of explicitly coupling the quantum and classical regions via electrostatic interactions as in Section 3.3, the QM part is also represented using the same classical model as the environment. One then performs two calculations with the classical model: one using a parametrization of the classical model based on the ground state and one using a parametrization based on the excited state of interest. Then, similar to the Δ -QM/MM-SCF of the previous section, the difference of the classical total energies is an energy correction to the respective vacuum excitation energy, cf. Equation (51). This way, the calculation of energy corrections is very fast and can be readily applied to, for instance, large molecular morphologies of amorphous materials, or is easily combined—depending on the details of the microelectrostatics model—with many of the available methods for efficient large-scale electrostatics methods like Particle or Particle-Mesh Ewald [69–71].

As an example for *GW* calculations using periodic embedding [73] in the subtractive sense, we show in Figure 9 the layer-resolved highest-occupied molecular orbital energy diagram of a thin film of 2-methyl-9,10-bis(naphthalen-2-yl)anthracene [72]. The studied film contains about 1000 molecules and the shown values for the respective layers are obtained by averaging over many individual embedded *GW* calculations.

Performing 1000 additive *GW*-BSE/MM as in Section 3.3 instead is orders of magnitude more computationally expensive. The disadvantage of using the subtractive method is that one needs classical microelectrostatics models for molecules both in their ground state (for the embedding region) and the excited state and that these models provide a sufficiently accurate representation of quantum mechanical electrostatic responses. In [72], for instance, this was checked for selected molecules in the bulk and at the surface of the film by comparing results from additive *GW*/MM and subtractively embedded *GW* calculations.

4 | Conclusion

In summary, we have explored in this review various strategies for building embedded many-body Green's function methods in application to complex molecular systems. These strategies differ in many aspects: from how the environment is represented (on a lower quantum-mechanical level, using a classical model with atomistic details, or by a polarizable continuum), to how the environment effects are included in the *GW*-BSE calculations (intrinsically via the screened Coulomb interaction W or extrinsically via a self-consistency in total energy calculations of electrostatically coupled regions). Despite their sometimes very fundamental differences, the presented example applications to molecular dimers, molecular crystals, solvated dye or DNA systems, macromolecules, and molecular thin films show that all the strategies contain the correct physics. Preference for a particular method might depend on the actual system under study, apparently more so regarding the choice of the environment model rather than how the effects of the model are included. Therefore, the careful parametrization of models for the embedding region is a common challenge for all approaches. These challenges are, however, not unique to embedded *GW*-BSE calculations and pertain to nearly all subsystem-type calculation that mix different levels of theory. More Green's function method specific challenges are related to the state-dependence of the environment response discussed above and, on a more technical level, extending the environment screening contribution beyond the static (zero-frequency) case. As the discussion of the example of the polarity-sensitive dye above has shown, many interesting chemical (or physical) processes involve not only a response of the electronic system but a change in structural properties of the molecular system. Eventually, this will require extending the embedded Green's function models to include nuclear dynamics.

Author Contributions

Gianluca Tirimbó: writing – original draft (equal), writing – review and editing (equal). **Vivek Sundaram:** writing – original draft (equal), writing – review and editing (equal). **Björn Baumeier:** writing – original draft (equal), writing – review and editing (equal).

Conflicts of Interest

The authors declare no conflicts of interest.

Data Availability Statement

Data sharing is not applicable to this article as no new data were created or analyzed in this study.

Related WIREs Articles

[GW method and Bethe-Salpeter equation for calculating electronic excitations](#)

References

1. M. S. Hybertsen and S. G. Louie, “First-Principles Theory of Quasiparticles: Calculation of Band Gaps in Semiconductors and Insulators,” *Physical Review Letters* 55, no. 13 (1985): 1418–1421.
2. M. S. Hybertsen and S. G. Louie, “Electron Correlation in Semiconductors and Insulators: Band Gaps and Quasiparticle Energies,” *Physical Review B* 34, no. 8 (1986): 5390–5413.
3. F. Bechstedt, *Many-Body Approach to Electronic Excitations. Springer Series in Solid-State Science*, 1st ed. (Berlin, Heidelberg: Springer, 2015).
4. P. Hohenberg and W. Kohn, “Inhomogeneous Electron Gas,” *Physics Review B* 136, no. 3 (1964): B864–B871.
5. W. Kohn and L. J. Sham, “Self-Consistent Equations Including Exchange and Correlation Effects,” *Physical Review A* 140, no. 4 (1965): A1133–A1138.
6. M. Röhlffing and S. G. Louie, “Electron-Hole Excitations and Optical Spectra From First Principles,” *Physical Review B* 62, no. 8 (2000): 4927–4944.
7. G. Kresse and J. Furthmüller, “Efficient Iterative Schemes for Ab Initio Total-Energy Calculations Using a Plane-Wave Basis Set,” *Physical Review B* 54, no. 16 (1996): 11169–11186.
8. J. Deslippe, G. Samsonidze, D. A. Strubbe, M. Jain, M. L. Cohen, and S. G. Louie, “A Massively Parallel Computer Package for the Calculation of the Quasiparticle and Optical Properties of Materials and Nanostructures,” *Computer Physics Communications* 183, no. 6 (2012): 1269–1289.
9. D. Sangalli, A. Ferretti, H. Miranda, et al., “Many-Body Perturbation Theory Calculations Using the Yambo Code,” *Journal of Physics: Condensed Matter* 31, no. 32 (2019): 325902.
10. T. D. Kühne, M. Iannuzzi, M. Del Ben, et al., “CP2K: An Electronic Structure and Molecular Dynamics Software Package – Quickstep: Efficient and Accurate Electronic Structure Calculations,” *Journal of Chemical Physics* 152, no. 19 (2020): 194103.
11. M. Röhlffing, “Electronic Excitations From a Perturbative LDA + GdW Approach,” *Physical Review B* 82, no. 20 (2010): 205127.
12. M. Marsili, E. Mosconi, F. De Angelis, and P. Umari, “Large-Scale \$GW\$-BSE Calculations With N3 Scaling: Excitonic Effects in Dye-Sensitized Solar Cells,” *Physical Review B* 95, no. 7 (2017): 075415.
13. L. Leppert, T. Rangel, and J. B. Neaton, “Towards Predictive Band Gaps for Halide Perovskites: Lessons From One-Shot and Eigenvalue Self-Consistent \$GW\$,” *Physical Review Materials* 3, no. 10 (2019): 103803.
14. R. I. Biega, Y. Chen, M. R. Filip, and L. Leppert, “Chemical Mapping of Excitons in Halide Double Perovskites,” *Nano Letters* 23, no. 17 (2023): 8155–8161.
15. B. Jeziorski and H. J. Monkhorst, “Coupled-Cluster Method for Multideterminantal Reference States,” *Physical Review A* 24, no. 4 (1981): 1668–1681.
16. T. Van Voorhis and M. Head-Gordon, “Benchmark Variational Coupled Cluster Doubles Results,” *Journal of Chemical Physics* 113, no. 20 (2000): 8873–8879.
17. F. A. Evangelista, “Alternative Single-Reference Coupled Cluster Approaches for Multireference Problems: The Simpler, the Better,” *Journal of Chemical Physics* 134, no. 22 (2011): 224102.
18. H. Appel, E. K. U. Gross, and K. Burke, “Excitations in Time-Dependent Density-Functional Theory,” *Physical Review Letters* 90, no. 4 (2003): 043005.

19. S. Kümmel, "Charge-Transfer Excitations: A Challenge for Time-Dependent Density Functional Theory That Has Been Met," *Advanced Energy Materials* 7, no. 16 (2017): 1700440.
20. X. Blase and C. Attaccalite, "Charge-Transfer Excitations in Molecular Donor-Acceptor Complexes Within the Many-Body Bethe-Salpeter Approach," *Applied Physics Letters* 99, no. 17 (2011): 171909.
21. B. Baumeier, D. Andrienko, and M. Rohlfing, "Frenkel and Charge-Transfer Excitations in Donor-Acceptor Complexes From Many-Body Green's Functions Theory," *Journal of Chemical Theory and Computation* 8, no. 8 (2012): 2790–2795.
22. S. Sharifzadeh, P. Darancet, L. Kronik, and J. B. Neaton, "Low-Energy Charge-Transfer Excitons in Organic Solids From First-Principles: The Case of Pentacene," *Journal of Physical Chemistry Letters* 4, no. 13 (2013): 2197–2201.
23. S. Körbel, P. Boulanger, I. Duchemin, X. Blase, M. A. L. Marques, and S. Botti, "Benchmark Many-Body GW and Bethe-Salpeter Calculations for Small Transition Metal Molecules," *Journal of Chemical Theory and Computation* 10, no. 9 (2014): 3934–3943.
24. M. J. van Setten, F. Caruso, S. Sharifzadeh, et al., "GW100: Benchmarking GOW0 for Molecular Systems," *Journal of Chemical Theory and Computation* 11, no. 12 (2015): 5665–5687.
25. D. Golze, M. Dvorak, and P. Rinke, "The GW Compendium: A Practical Guide to Theoretical Photoemission Spectroscopy," *Frontiers in Chemistry* 7 (2019): 7.
26. D. Jacquemin, I. Duchemin, and X. Blase, "Benchmarking the Bethe-Salpeter Formalism on a Standard Organic Molecular Set," *Journal of Chemical Theory and Computation* 11, no. 7 (2015): 3290–3304.
27. B. Baumeier, M. Rohlfing, and D. Andrienko, "Electronic Excitations in Push-Pull Oligomers and Their Complexes With Fullerene From Many-Body Green's Functions Theory With Polarizable Embedding," *Journal of Chemical Theory and Computation* 10, no. 8 (2014): 3104–3110.
28. A. Förster and L. Visscher, "Quasiparticle Self-Consistent GW-Bethe-Salpeter Equation Calculations for Large Chromophoric Systems," *Journal of Chemical Theory and Computation* 18, no. 11 (2022): 6779–6793.
29. C. Daday, C. König, O. Valsson, J. Neugebauer, and C. Filippi, "State-Specific Embedding Potentials for Excitation-Energy Calculations," *Journal of Chemical Theory and Computation* 9, no. 5 (2013): 2355–2367.
30. E. D. Hedegård and M. Reiher, "Polarizable Embedding Density Matrix Renormalization Group," *Journal of Chemical Theory and Computation* 12, no. 9 (2016): 4242–4253.
31. X. Wen, D. S. Graham, D. V. Chulhai, and J. D. Goodpaster, "Absolutely Localized Projection-Based Embedding for Excited States," *Journal of Chemical Theory and Computation* 16, no. 1 (2020): 385–398.
32. J. M. H. Olsen, C. Steinmann, K. Ruud, and J. Kongsted, "Polarizable Density Embedding: A New QM/QM/MM-Based Computational Strategy," *Journal of Physical Chemistry* 119, no. 21 (2015): 5344–5355.
33. J. Tomasi, B. Mennucci, and R. Cammi, "Quantum Mechanical Continuum Solvation Models," *Chemical Reviews* 105, no. 8 (2005): 2999–3094.
34. B. Mennucci, S. Caprasecca, and C. A. Guido, "Chapter Four – Computational Studies of Environmental Effects and Their Interplay With Experiment," in *Advances in Physical Organic Chemistry*, vol. 50, eds. I. H. Williams and N. H. Williams (Amsterdam, The Netherlands: Academic Press, 2016), 203–241.
35. B. Mennucci and R. Cammi, *Continuum Solvation Models in Chemical Physics* (Chichester: John Wiley & Sons, Ltd, 2007).
36. D. R. Hartree, "The Wave Mechanics of an Atom With a Non-Coulomb Central Field. Part II. Some Results and Discussion," *Mathematical Proceedings of the Cambridge Philosophical Society* 24, no. 1 (1928): 111–132.
37. J. C. Slater, "The Self Consistent Field and the Structure of Atoms," *Physics Review* 32, no. 3 (1928): 339–348.
38. A. Seidl, A. Görling, P. Vogl, J. A. Majewski, and M. Levy, "Generalized Kohn-Sham Schemes and the Band-Gap Problem," *Physical Review B* 53 (1996): 3764–3774.
39. L. Hedin, "New Method for Calculating the One-Particle Green's Function With Application to the Electron-Gas Problem," *Physical Review A* 139, no. 3 (1965): A796–A823.
40. L. Hedin and S. Lundqvist, "Effects of Electron-Electron and Electron-Phonon Interactions on the One-Electron States of Solids," in *Solid State Physics*, vol. 23, eds. F. Seitz, D. Turnbull, and H. Ehrenreich (Cambridge: Academic Press, 1970), 1–181.
41. M. van Schilfgaarde, T. Kotani, and S. Faleev, "Quasiparticle Self-Consistent \$GW\$ Theory," *Physical Review Letters* 96, no. 22 (2006): 226402.
42. A. Stan, N. E. Dahlen, and R. van Leeuwen, "Levels of Self-Consistency in the GW Approximation," *Journal of Chemical Physics* 130, no. 11 (2009): 114105.
43. K. Eichkorn, O. Treutler, H. Öhm, M. Häser, and R. Ahlrichs, "Auxiliary Basis Sets to Approximate Coulomb Potentials," *Chemical Physics Letters* 240, no. 4 (1995): 283–290.
44. L. Cao and U. Ryde, "On the Difference Between Additive and Subtractive QM/MM Calculations," *Frontiers in Chemistry* 6 (2018): 89.
45. F. R. Manby, M. Stella, J. D. Goodpaster, and T. F. I. Miller, "A Simple, Exact Density-Functional-Theory Embedding Scheme," *Journal of Chemical Theory and Computation* 8, no. 8 (2012): 2564–2568.
46. C. R. Jacob and J. Neugebauer, "Subsystem Density-Functional Theory," *WIREs Computational Molecular Science* 4, no. 4 (2014): 325–362.
47. C. R. Jacob and J. Neugebauer, "Subsystem Density-Functional Theory (Update)," *WIREs Computational Molecular Science* 14, no. 1 (2024): e1700.
48. G. Senatore and K. R. Subbaswamy, "Density Dependence of the Dielectric Constant of Rare-Gas Crystals," *Physical Review B* 34, no. 8 (1986): 5754–5757.
49. M. D. Johnson, K. R. Subbaswamy, and G. Senatore, "Hyperpolarizabilities of Alkali Halide Crystals Using the Local-Density Approximation," *Physical Review B* 36, no. 17 (1987): 9202–9211.
50. P. Cortona, "Self-Consistently Determined Properties of Solids Without Band-Structure Calculations," *Physical Review B* 44, no. 16 (1991): 8454–8458.
51. T. A. Wesolowski and A. Warshel, "Frozen Density Functional Approach for Ab Initio Calculations of Solvated Molecules," *Journal of Physical Chemistry* 97, no. 30 (1993): 8050–8053.
52. T. A. Wesolowski and J. Weber, "Kohn-Sham Equations With Constrained Electron Density: An Iterative Evaluation of the Ground-State Electron Density of Interacting Molecules," *Chemical Physics Letters* 248, no. 1 (1996): 71–76.
53. J. Tölle, T. Deilmann, M. Rohlfing, and J. Neugebauer, "Subsystem-Based GW/Bethe-Salpeter Equation," *Journal of Chemical Theory and Computation* 17, no. 4 (2021): 2186–2199.
54. J. Tölle, T. Deilmann, M. Rohlfing, and J. Neugebauer, "Correction to 'Subsystem-Based GW/Bethe-Salpeter Equation,'" *Journal of Chemical Theory and Computation* 19, no. 9 (2023): 2699–2702.
55. I. Duchemin, D. Jacquemin, and X. Blase, "Combining the GW Formalism With the Polarizable Continuum Model: A State-Specific Non-Equilibrium Approach," *Journal of Chemical Physics* 144, no. 16 (2016): 164106.

56. R. E. Bulo, B. Ensing, J. Sikkema, and L. Visscher, "Toward a Practical Method for Adaptive QM/MM Simulations," *Journal of Chemical Theory and Computation* 5, no. 9 (2009): 2212–2221.
57. J. Li, G. D'Avino, I. Duchemin, D. Beljonne, and X. Blase, "Accurate Description of Charged Excitations in Molecular Solids From Embedded Many-Body Perturbation Theory," *Physical Review B* 97, no. 3 (2018): 035108.
58. P. Drude, "Zur Elektronentheorie Der Metalle," *Annals of Physics* 306, no. 3 (1900): 566–613.
59. M. Dressel and M. Scheffler, "Verifying the Drude Response," *Annals of Physics* 518, no. 7–8 (2006): 535–544.
60. A. K. Rappe and W. A. I. Goddard, "Charge Equilibration for Molecular Dynamics Simulations," *Journal of Physical Chemistry* 95, no. 8 (1991): 3358–3363.
61. D. Ongari, P. G. Boyd, O. Kadioglu, A. K. Mace, S. Keskin, and B. Smit, "Evaluating Charge Equilibration Methods To Generate Electrostatic Fields in Nanoporous Materials," *Journal of Chemical Theory and Computation* 15, no. 1 (2019): 382–401.
62. J. Applequist, J. R. Carl, and K. K. Fung, "Atom Dipole Interaction Model for Molecular Polarizability. Application to Polyatomic Molecules and Determination of Atom Polarizabilities," *Journal of the American Chemical Society* 94, no. 9 (1972): 2952–2960.
63. B. T. Thole, "Molecular Polarizabilities Calculated With a Modified Dipole Interaction," *Chemical Physics* 59, no. 3 (1981): 341–350.
64. P. T. van Duijnen and M. Swart, "Molecular and Atomic Polarizabilities: Thole's Model Revisited," *Journal of Physical Chemistry* 102, no. 14 (1998): 2399–2407.
65. S. Baral, M. Phillips, H. Yan, et al., "Ultrafast Formation of the Charge Transfer State of Prodan Reveals Unique Aspects of the Chromophore Environment," *Journal of Physical Chemistry B* 124, no. 13 (2020): 2643–2651.
66. E. V. Tsiper and Z. G. Soos, "Charge Redistribution and Polarization Energy of Organic Molecular Crystals," *Physical Review B* 64, no. 19 (2001): 195124.
67. G. D'Avino, L. Muccioli, F. Castet, et al., "Electrostatic Phenomena in Organic Semiconductors: Fundamentals and Implications for Photovoltaics," *Journal of Physics: Condensed Matter* 28, no. 43 (2016): 433002.
68. L. Galleni, A. Meulemans, F. S. Sajadian, et al., "Peak Broadening in Photoelectron Spectroscopy of Amorphous Polymers: The Leading Role of the Electrostatic Landscape," *Journal of Physical Chemistry Letters* 15, no. 3 (2024): 834–839.
69. T. Darden, D. York, and L. Pedersen, "Particle Mesh Ewald: An N $\log(N)$ Method for Ewald Sums in Large Systems," *Journal of Chemical Physics* 98 (1993): 10089–10092.
70. J. J. Cerdà, V. Ballenegger, O. Lenz, and C. Holm, "P3M Algorithm for Dipolar Interactions," *Journal of Chemical Physics* 129, no. 23 (2008): 234104.
71. A. Arnold and C. Holm, "Efficient Methods to Compute Long-Range Interactions for Soft Matter Systems," in *Advanced Computer Simulation Approaches for Soft Matter Sciences II. Advances in Polymer Science*, eds. C. Holm and K. Kremer (Berlin, Heidelberg: Springer Berlin Heidelberg, 2005), 59–109.
72. G. Tirimbò, X. de Vries, C. H. L. Weijtens, et al., "Quantitative Predictions of Photoelectron Spectra in Amorphous Molecular Solids From Multiscale Quasiparticle Embedding," *Physical Review B* 101, no. 3 (2020): 035402.
73. C. Poelking, M. Tietze, C. Elschner, et al., "Impact of Mesoscale Order on Open-Circuit Voltage in Organic Solar Cells," *Nature Materials* 14, no. 4 (2015): 434–439.